University of South-Eastern Norway
Faculty of Technology, Natural Sciences and Maritime Sciences

Master's Thesis

Study programme: Master of Science in Micro and Nano Systems Technology

Spring 2023

Tasfia Nowshin Farook

Optimized growth of iCL-CNT on a microstructured Al substrate for high energy density supercapacitors

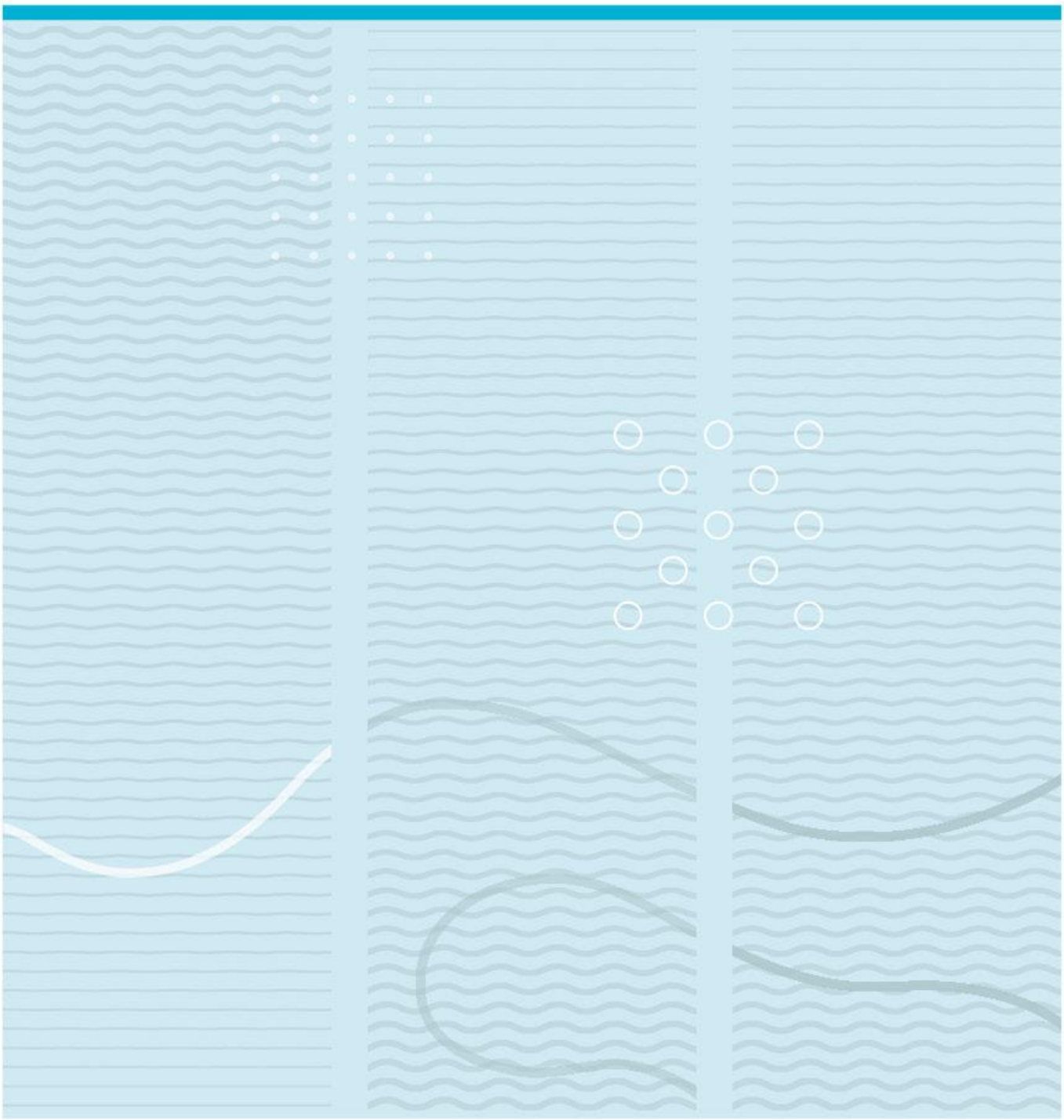

University of South-Eastern Norway
Faculty of Technology, Natural Sciences and Maritime Sciences
Department of Microsystems.
Raveien 215
NO-3184 Borre, Norway

http://www.usn.no

Abstract

This study presents the synthesis of millimeter-tall interconnected cross-linked carbon nanotubes (iCL-CNTs) with high specific capacitance, grown directly on pre-etched Aluminium (Al) substrates. Atmospheric pressure chemical vapor deposition (APCVD) was performed both with and without water assistance at 600℃, utilizing a 20-minute optimized synthesis time and Nickel sulfate ($NiSO_4$) solution coating as the catalyst layer. The growth mechanism of CNTs was highly sensitive to gas ratios, necessitating a systematic investigation of the optimal gas ratios and other CVD conditions. The key to achieving high mass loading of CNTs was found to be the control of $NiSO_4$ volume under optimized gas flow rates and synthesis time. Water-assisted CVD, under optimal gas conditions and synthesis time, yielded millimeter-tall iCL-CNTs with an areal capacitance of 1486mF/cm². Remarkably, under the same parameters, without water assistance, areal capacitance increased significantly to 2471mF/cm². The effects of varying synthesis times on the adhesiveness of the grown CNTs were systematically studied and this study suggests that $NiSO_4$ could be a promising catalyst option, requiring more exploration.

Foreword

This thesis represents the culmination of my master's program in Micro and Nano Systems Technology at the University of South-Eastern Norway(USN), and its successful completion would not have been possible without the support and guidance of several people along the way. My supervisor, Dr. Xuyuan Chen, and co-supervisor, Dr. Raghunandan Ummethala, have provided me with unwavering support and invaluable guidance throughout the completion of my thesis. Their expertise and encouragement have been shaping the core understanding of my research work.

I am also thankful to Per Ohlckers and nanoCaps for their collaboration on this thesis, which has allowed me to acquire a deeper understanding of the supercapacitor industry as well as novel battery technologies. Their contributions have been significant in expanding my knowledge and refining my abilities in this discipline.

Special thanks are due to our lab engineers, for their continuous support and assistance during laboratory work.

Lastly, I would like to dedicate this thesis to my father, who has always believed in me and encouraged me to pursue higher education abroad. His unwavering faith in my abilities has been my driving force throughout this journey. Unfortunately, he is now an Alzheimer's patient and may not be able to fully comprehend my achievements, but his influence remains an integral part of my success. This thesis is a testament to his love and support, and I dedicate it to him with immense gratitude and appreciation.

<Vestfold, Norway/22/05/2023>

<Tasfia Nowshin Farook>

Contents

1 Introduction

The exponential growth in global energy demand is being powered by rapid industrialization, urbanization, and technological advancements, which are being observed worldwide. The increase in demand has led to the exploration and creation of energy storage systems that are efficient, environmentally friendly, and socially responsible. Energy storage devices are a highly promising and powerful technology with significant environmental implications that have a profound impact on the advancement of our civilization's capabilities and quality of life. Electrochemical capacitors function as energy storage mechanisms, exhibiting important levels of effectiveness and efficiency. They exhibit an elongated lifespan, higher energy density, and the capacity for rapid charging and discharging. The utilization of capacitor technology is perceived as a propitious strategy for the storage of electrical energy. Researchers globally are actively engaged in enhancing the energy density of electrochemical capacitors to meet the growing need for energy storage applications [1].

Supercapacitors have become an effective alternative for energy storage applications, built on the promising qualities of electrochemical capacitors. Supercapacitors, also known as electric double-layer capacitors (EDLC) or ultracapacitors, possess a high energy storage capacity and low internal resistance. They can store and discharge energy at comparatively higher rates than batteries. This is due to the energy storage mechanism that involves a straightforward charge separation at the interface between the electrode and the electrolyte. A supercapacitor is composed of a pair of electrodes, an electrolyte, and a separator that serves to electrically isolate the two electrodes [2]. In a conventional capacitor, two metallic plates (electrodes) are separated by a dielectric substance. The accumulation of electrons at a specific electrode upon the application of voltage leads to the storage of electrical charge. The sole distinction lies in the utilization of an electrolytic solution as the intermediary substance in a supercapacitor, as opposed to a dielectric [3]. Supercapacitors can be positioned between conventional capacitors and batteries, as they offer higher energy densities than conventional capacitors, but lower power densities. Additionally, they exhibit superior power density and cyclability compared to batteries, although their energy density is comparatively lower. Supercapacitors are particularly attractive for use in scenarios that require high power, low energy, and

frequent charge/discharge cycles. Illustrative instances of such applications comprise regenerative braking systems in fully electric or heavy hybrid vehicles with multiple daily start/stop cycles (e.g., city transit buses and garbage trucks), energy management in microgrids or stand-alone systems, portable consumer electronics, AC line filtering, water desalination systems, memory backup systems, emergency airplane doors, wind turbine blade pitch systems, and seaport cranes [4]–[6].

1.1 Electrode materials for supercapacitors

Here a selection of electrode material plays a crucial role for supercapacitors. Remarkable power and energy densities have been achieved in laboratory-scale devices owing to a number of innovations combining different electrode materials and combinations. The utilization of carbon materials, in their diverse configurations, as electrode materials for supercapacitors is prevalent owing to their higher surface area, cost-effective nature, and widespread accessibility. Thus, the capacitance is predominantly conditional upon the extent of the surface area that is available for the electrolyte ions to access. The electrochemical performance is influenced by several important factors, namely the specific surface area, pore shape and structure, pore size distribution, surface functionality, and electrical conductivity. The improvement of charge accumulation capacity at the electrode-electrolyte interface is a direct consequence of a high specific surface area exhibited by carbon materials [7] .

Activated carbon is mostly employed to expand these regions due to its porous nature and the presence of multiple pores on its surface, which enables it to cover a wide surface area [1], [8], [9]. Due to their cost-effectiveness and diverse range of pre-existing forms including powders, felts, composites, mats, monoliths, and foils, carbon materials have found extensive usage in the realm of supercapacitor applications. The efficacy of charging the electrical double layer is contingent upon the utilization of materials possessing a substantial surface area and pores that are tailored to the dimensions of ions. This is a critical factor in the performance of supercapacitors. The utility of charging the electrical double layer (EDL) is limited to the electrochemically available surface area. However, the presence of small mesopores can be beneficial for effective dynamic charge propagation. It is anticipated that a carbon material possessing a high surface area, featuring narrow pores measuring less than 1nm, and exhibiting a well-proportioned

micro/mesoporosity will yield optimal performance. Therefore, it is essential to exercise rigorous control over the carbonization and activation procedures to produce carbon materials that are optimized. Although conventional carbons possess a large specific surface area and are relatively inexpensive, their potential for use in EDLC applications is restricted due to their wide distribution of pore sizes and randomly connected pores, which ultimately restricts both their charge storage capacity and rate capability [10].

1.2 Carbon nanotubes for improved energy density supercapacitors

Research in this area has focused heavily on bettering the low energy density characteristics of supercapacitors while yet maintaining their high-power density and cyclability. One of the most efficient ways to address the problem of low energy density is to develop new electrode materials for supercapacitors. To overcome the constraints associated with traditional active carbon supercapacitors, scholars are investigating alternative carbon materials as a substitute for active carbon. To accomplish this objective, cutting-edge nanomaterials, particularly carbon nanotubes (CNTs), are being utilized to fabricate electrodes that extend energy-power capabilities. The distinctive pore structure, remarkable mechanical and thermal stability, and exceptional electrical properties of CNTs have rendered them a subject of considerable attention as electrode materials for supercapacitors. CNTs can be produced via catalytic decomposition of specific hydrocarbons. By carefully manipulating various parameters, it is possible to generate nanostructures with varied conformations and controlled crystalline structures. Compared to alternative carbon-based electrodes, CNTs exhibit interconnected mesopores that enable a consistent distribution of charge, leading to the efficient utilization of almost the entire available surface area. CNTs exhibit superior electrochemical stability compared to activated carbon due to their mesoporous network, which facilitates the diffusion of electrolyte ions, leading to a reduction in equivalent series resistance (ESR). In addition, the exceptional mechanical resilience and porous tubular architecture of carbon nanotubes make them a highly suitable substrate for hosting active materials [7], [10].

1.3 Objective

The main objective of this study is to optimize the fabrication process of iCL-CNTs on industrially pre-etched aluminium (Al) foil to create economically viable and high-functioning electrodes for supercapacitors. iCL-CNTs are a type of CNTs that are randomly oriented and chemically cross-linked with one another through functional groups. The cross-linked networks demonstrate improved mechanical, electrical, and thermal characteristics. Upon cross-linking, the CNTs establish robust intermolecular connections, thereby creating a highly effective route for the transportation of charge carriers, including electrons and holes, throughout the network. The cross-links facilitate the movement of charge carriers between carbon nanotubes by reducing resistance and barriers, thereby enhancing the material's electrical conductivity [11]. To attain this objective, it is necessary to investigate the optimal combination of gases and synthesis durations for the purpose of producing iCL-CNTs that demonstrate particular characteristics such as significant interconnectivity, crosslinking, robust adhesion, and a higher mass loading of CNTs. It is important to mention that an electrode possessing a higher quantity of active mass of CNTs can store a larger amount of energy, resulting in a higher specific capacitance. This attribute holds significant value in the context of commercial applications. Optimizing the synthesis time would not only result in a decrease in the overall production cost, but it would also improve the process's scalability for industrial applications. To reduce production costs and uphold the quality of synthesized iCL-CNTs, this study suggests implementing the dip or drop coating technique for sample preparation. It entails the application of a liquid suspension of the catalyst material onto a substrate, succeeded by the evaporation of the solvent.

1.4 Research approach

The present study seeks to carefully investigate and enhance the fabrication process of supercapacitor electrodes utilizing iCL-CNTs. The methodology that will be utilized involves conducting a systematic literature review to establish a robust basis of pre-existing knowledge. A design for an experimental arrangement will be formulated with the aim of optimizing the synthesis parameters, substrate, and catalyst selection for the growth of iCL-CNTs. This will be followed by a catalyst particle deposition process to

ensure uniformity and higher mass loading. The fabricated electrodes will be subjected to a thorough analysis using advanced characterization techniques. The assessment of electrochemical performance will involve the utilization of cyclic voltammetry (CV) and ESR techniques to evaluate the specific capacitance. The data acquired will undergo analysis with the aim of optimizing the fabrication process, thereby improving energy density as electrodes based on iCL-CNTs for supercapacitors. The study will conclude with a comprehensive report that will present the findings, conclusions, and future research directions. This will contribute to the advancement of supercapacitor technology.

2 Theoretical Background

2.1 Supercapacitors

Supercapacitors are gaining popularity as potential substitutes for conventional battery sources. The supercapacitor is characterized by a capacitance rating in farads, which is significantly greater than that of the electrolytic capacitor. Supercapacitors are found to be more effective as a low-maintenance memory backup that can bridge short power interruptions, as compared to functioning solely as an independent energy storage device. EDLC and pseudo-capacitance are the two primary storage mechanisms that differentiate them from conventional capacitors and batteries. The composition of an EDLC cell comprises a pair of electrodes, a separator, and an electrolyte. Activated carbon is a commonly utilized material to produce electrodes, owing to its exceptional electrical conductivity and extensive surface area. The metallic collector foils establish electrical connectivity between the electrodes and the terminals. To avoid short circuits, an ion-permeable membrane, commonly referred to as a separator, is interposed between the electrodes. The cellular structure is frequently contorted into a cylindrical or rectangular configuration and contained within an enclosure made of aluminium, either in the form of a container or a rectangular casing. The cell is infused with an electrolyte that can either be organic or aqueous, contingent upon the specific application, power requisites, voltage spectrum, and temperature parameters. The exterior casing is hermetically sealed to guarantee its integrity. Upon application of a voltage, the ions present in the electrolyte undergo migration across the separator and accumulate at the interface between the electrodes and the electrolyte. This results in the formation of charged layers that are separated by a certain distance. The phenomenon of charge separation gives rise to the double layer capacitance, which is characterized by high capacitance values that arise from the contrast of a large surface area and a small distance between the charged layers (Figure 2-1 (b)).

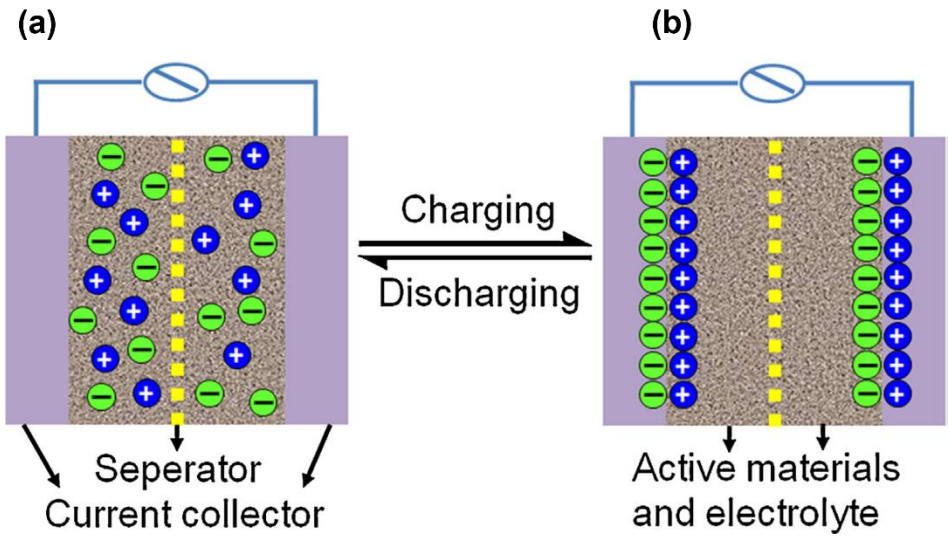

Figure 2-1: Schematic illustration of charging/discharging process in supercapacitor (a) pseudo-capacitance (b) EDLC [12].

The operational mechanism of pseudo-capacitance in supercapacitors is predicated on the reversible redox reactions that occur at the interface between the electrode and electrolyte. Pseudo-capacitive materials, comprising of conductive polymers or metal oxides, exhibit electrochemical reactions by because of electron transfer during the process of charge and discharge. The reactions facilitate the potential for ions to be stored in a reversible manner or for the insertion of ions into the material of the electrode. During the process of charging, the electroactive elements present in the electrode undergo oxidation, leading to the storage of ions and the release of electrons. Therefore, there is an accumulation of charge on the surface of the electrode. During the process of discharging, electroactive elements experience a reduction reaction, resulting in the release of stored ions and the acceptance of electrons (Figure 2-1 (a)).

The performance of supercapacitors relies on the physical properties of the electrode and electrolyte materials. Activated carbon electrodes face limitations in terms of low mesoporosity and electrolyte accessibility, resulting in restricted capacitance and energy density. Additionally, they exhibit poor electrical conductivity, leading to high internal resistance and low power density. To address these challenges, carbon nanomaterials such as graphene and CNTs are promising alternatives due to their large surface area, high mesoporosity, electrolyte accessibility, and favourable electrical properties. These

nanomaterials have the potential to enhance supercapacitor performance by improving energy density and power density [2], [12] .

2.2 Carbon nanotubes: structure and properties

CNTs are an intriguing nanomaterial with special mechanical, thermal, and electrical characteristics that make them very fascinating for use in a variety of applications. Since their discovery by Sumio Iijima in 1991 [13], they have been the subject of intensive research. With their distinctive features, CNTS, which are cylindrical structures comprised of carbon atoms organized in a tubular pattern, are potential materials for use in industries including electronics, energy, and materials research. Understanding the background theory of CNTs is essential to fully appreciate their potential and to develop novel applications for them. CNTs are a form of carbon characterized by a diameter in the nanometre range and a length in the micrometre range. The atomic arrangement in hexagonal patterns is analogous to that of graphite. CNTs possess a structure that comprises a cylindrical graphitic sheet, commonly referred to as graphene, that is rolled into a cylinder with a diameter that measures in the nanometre scale. CNTs are an emerging member of the carbon allotrope family, occupying a position between fullerenes and graphite. CNTs are classified as a member of the structural group of fullerenes, which encompasses buckyballs as well. While buckyballs exhibit a spherical morphology, CNTs possess a cylindrical structure [14]. CNTs have classified based on the number of tubes present in rolled-up graphene sheets and chirality (Chirality means that an object or molecule cannot be superimposed on its mirror image by any translations or rotations). There are mainly two types of CNTs Single-walled (SWCNTs) and Multi-walled (MWCNTs) based on the number of tubes present. SWCNT is essentially a seamless cylinder formed by rolling a single layer of graphite, also known as a graphene layer. These long-wrapped sheets of graphene give rise to SWCNTs, which are nearly one-dimensional structures due to their length to diameter ratio of about 1000 or more. Most SWCNTs possess a diameter of approximately 1nm. It is worth noting that SWCNTs consist of two distinct regions with different physical and chemical properties - the sidewall of the tube and the end cap of the tube, as pointed out by Iijima and Ichihashi in 1993 [15]. The categorization of SWCNTs is based on the specific wrapping of the

graphene layer into a cylindrical shape, resulting in three distinct types: armchair, chiral, and zigzag. The chiral vector, denoted as (n, m), defines the structure of a SWCNT. The aforementioned indices exert a considerable impact on the electrical characteristics of the nanotube [16].MWCNTs are composed of concentric SWCNTs with different diameters. The mentioned structures are composed of multiple layers of graphite that have been rolled into a tubular configuration. It is significant that these structures exhibit notable distinctions from SWCNTs in relation to their length and diameter. Thus, the characteristics of MWCNTs differ from those of SWCNTs. For the formation of MWCNTs, there are two structural models: the Russian Doll model and the Parchment model. This refers to a situation in which a CNTs contains a nanotube with a smaller diameter within it, while the external nanotube has a larger diameter. In contrast, the Parchment method involves the repeated rolling of a single graphene layer, similar to how paper scrolls are rolled [14].

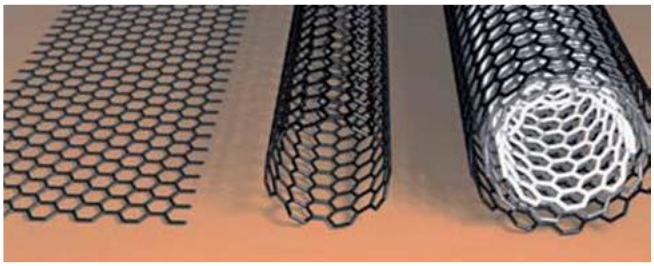

Figure 2-2: Graphical representation of graphene sheet, SWCNT, and MWCNT [17].

CNTs are a distinct form of carbon allotropes that show a range of exceptional properties, rendering them highly appealing for diverse applications. They exhibit a high level of electrical and thermal conductivity, which makes them valuable for utilization in fields such as electronics and energy storage systems. CNTs possess a high degree of thermal conductivity, which renders them well-suited for deployment in scenarios that necessitate high power densities and rapid charge/discharge rates, owing to their ability to facilitate efficient heat dissipation. The previously mentioned characteristic of CNT based supercapacitor electrodes enables efficient thermal management during high-power operation, thereby mitigating thermal degradation and enhancing the overall performance and safety of the device. CNTs exhibits excellent electric conductivity by allowing efficient movement of electrons along the length of the nanotubes and this

higher mobility of electron ensures that the entire surface area of the electrode is effectively utilize for charge storage. The present study refers to iCL-CNTs which are synthesized via the chemical cross-linking of discrete carbon nanotubes utilizing functional groups. The mentioned method of cross-linking results in the formation of a network structure that is interconnected in three dimensions. The intermolecular connections facilitated by cross-links among CNTs enable efficient transportation of charge carriers, such as electrons, across the network with robustness. The increased level of interconnectivity facilitates a decrease in resistance, ultimately concluding in an increase of electrical conductivity. The process of cross-linking enhances the thermal conductivity of the material by facilitating more efficient thermal transport pathways throughout the network [18], [19].

The versatile nature of CNTs, coupled with their diminutive size, makes them a promising material for diverse applications across various domains such as electronics, energy storage, biomedicine, and materials science.

2.3 Chemical vapor deposition (CVD) process

The method of electric arc discharge, which was one of the first techniques employed to produce CNTs, was originally utilized by R. Bacon during the 1960s for the purpose of synthesizing carbon fibers that were commonly referred to as whiskers. Subsequently, in the year 1990, Krätschmer and Huffman modified this methodology to efficiently produce fullerenes, and it was afterward upgraded to produce MWCNTs and SWCNTs. CNTs production has been successfully achieved through alternative techniques, including laser evaporation/ablation and chemical vapor deposition (CVD). The process of laser evaporation exhibits certain technical similarities with the arc discharge method, however, there are significant variations in the quality and purity of the resulting product between the two methods. At present, arc discharge and diverse forms of CVD are considered as the most auspicious and extensively employed methodologies for the extensive-scale manufacturing of CNTs and associated substances. CVD technique is widely acknowledged as a suitable method for the synthesis of CNTs owing to its simplicity and cost-effectiveness. CVD presents several benefits, such as its potential for large-scale manufacturing, the utilization of diverse hydrocarbons and substrates, and the capacity to generate diverse configurations and structures of CNTs. Low-Pressure

CVD (LPCVD) and APCVD are the two main varieties of CVD processes. The process of CNTs synthesis through CVD is predicated on the catalytic decomposition of gases containing carbon on catalysts. These catalysts are typically composed of thin films or deposited nanoparticles of transition metals, such as iron (Fe), cobalt (Co), or nickel (Ni), or their alloys.

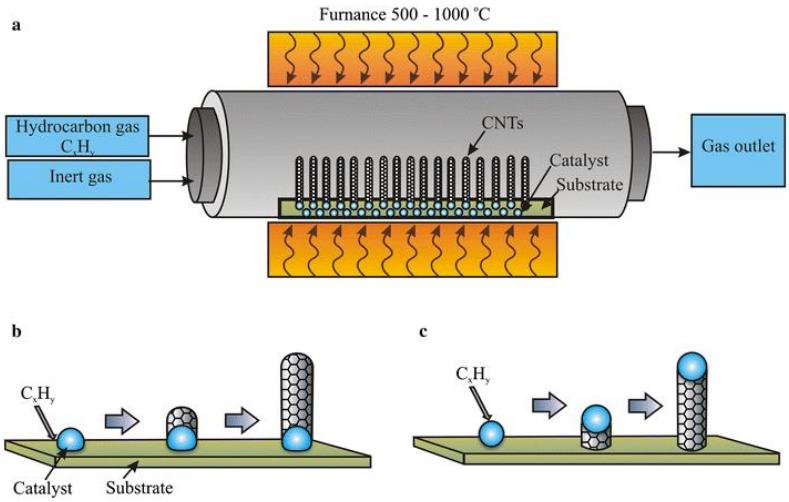

Figure 2-3: Schematic representation of CVD Process (a) CVD furnace/reactor (b) CNTs synthesis during CVD process [20].

The material that is being supported is introduced into a cylindrical vessel known as a tubular reactor for the purpose of facilitating the growth process. Upon achieving the requisite reaction temperature range of 600-1200℃, a blend of hydrocarbon gas and process gas undergoes a reaction within a chamber, facilitated by a metallic catalyst's surface, for a predetermined period. During the decomposition process of the carbon precursor, the catalyst particles present in the reactor facilitate the growth of CNTs. Upon reaching ambient temperature, the CNTs can be retrieved from the reactor walls and support surface [17], [21]–[23].

2.4 Substrate for CNT growth

The utilization of catalysts necessitates the use of a suitable substrate material for the growth of CNTs. Various substrates, including wafer of silicon, silicon carbide, quartz, silica. The film alumina, aluminium(Al), iron(Fe), iron(Fe)–nickel(Ni) alloy, iron(Fe)–terbium(Tb) alloy, nickel(Ni), iron(Fe)–molybdenum(Mo), molybdenum(Mo) powder, cobalt(Co), and cobalt(Co)–copper (Cu), are used in CVD for the fabrication of CNTs, among other materials. The substrate material exerts an influence on both the quantity and quality of the CNTs that are produced. The substrate material, its surface morphology, and textural attributes are crucial factors in the process as they serve as a support medium and interact with the catalyst and growth environment. The catalyst may undergo chemical and physical interactions with the substrate constituents. The stabilization of catalyst particle size distribution during CNT synthesis can be attributed to physical interactions, namely Van-der-Waals and electrostatic forces, which impede the movement of catalyst particles on the support material. The mentioned interactions have the potential to mitigate thermally induced diffusion and sintering phenomena of metallic particles on the underlying substrate. During CNT development, it is observed that the size distribution of the catalyst particles can be sustained through the chemical interactions that occur between the catalyst particles and the surface groups of the substrate. The utilization of a micro structured surface can serve as a scaffold template to regulate the growth of iCL-CNTs on a metal film substrate. This process is achieved through the utilization of metal nanoparticles as catalysts, which are supported on the micro structured surface. A variety of metals, including aluminium, copper, nickel, titanium, chromium, and stainless steel, can serve as suitable substrates for metal film deposition. However, it is important to regulate the presence of impurities in the metal to achieve optimal leakage current [21], [24].

2.5 Catalyst nanoparticles for CNT growth

The role of catalysts is of great significance in enhancing the desired characteristics of CNTs, thereby leading to an improvement in their yield and quality. Catalyst nanoparticles serve as nucleation centers for the growth of CNTs, thus playing a important role in the formation of the resultant nanotube. The catalyst serves the purpose of facilitating the

decomposition of hydrocarbons at temperatures lower than the temperature required for spontaneous decomposition of hydrocarbons through heat, leading to the formation of CNTs via nucleation. Transition metal nanoparticles are commonly utilized as catalysts in the CVD process for synthesizing CNTs. The diameter of the tube is typically determined by the size of the catalyst particle. Specifically, when the catalyst particle is small, SWCNTs tend to form, whereas larger particles, typically tens of nanometers in size, endorse the formation of MWCNTs. Currently, there exists a lack of satisfactory control over the diameter, length, and chirality of CNTs in a singular process, owing to an incomplete comprehension of the catalyst's function in nanotube nucleation and growth. Transition metals, specifically Fe, Co, and Ni, in the form of nanoparticles have been observed to exhibit superior catalytic activity. This can be attributed to the fact that these metals possess high solubility for carbon at elevated temperatures. The metals in question exhibit a high diffusion rate of carbon. The selection of a catalyst is an essential consideration that impacts the growth of CNTs [21], [22], [25].

2.6 Growth mechanism of CNTs

The process of CNT formation can be explained through the utilization of CVD in tandem with a catalyst. A surface upon which a chemical reaction takes place is covered by a slender coating of a substance that accelerates the reaction, typically a transition metal like Fe, Co, or Ni. Subsequently, the substrate is introduced into a reactor chamber and subjected to a carbon-based gas, such as acetylene or ethylene, which undergoes decomposition on the surface of the catalyst. The surface of the catalyst becomes saturated with carbon, resulting in the formation of microscopic carbon clusters on its surface. As carbon atoms or molecules are added to the cluster, it undergoes expansion and ultimately takes on a cylindrical shape, resulting in the formation of a CNTs. The growth of nanotubes is commonly oriented parallel to the catalyst particle's axis. The gradual coverage of the catalyst particle by carbon compounds as CNTs grow results in a reduction of its activity. To maintain the expansion of CNTs, it is imperative to revive the catalyst through the elimination of carbon compounds that have formed on its surface. The above procedure is achieved through the introduction of hydrogen gas into the reactor. This gas undergoes a reaction with carbon compounds, resulting in their removal from the surface of the catalyst.

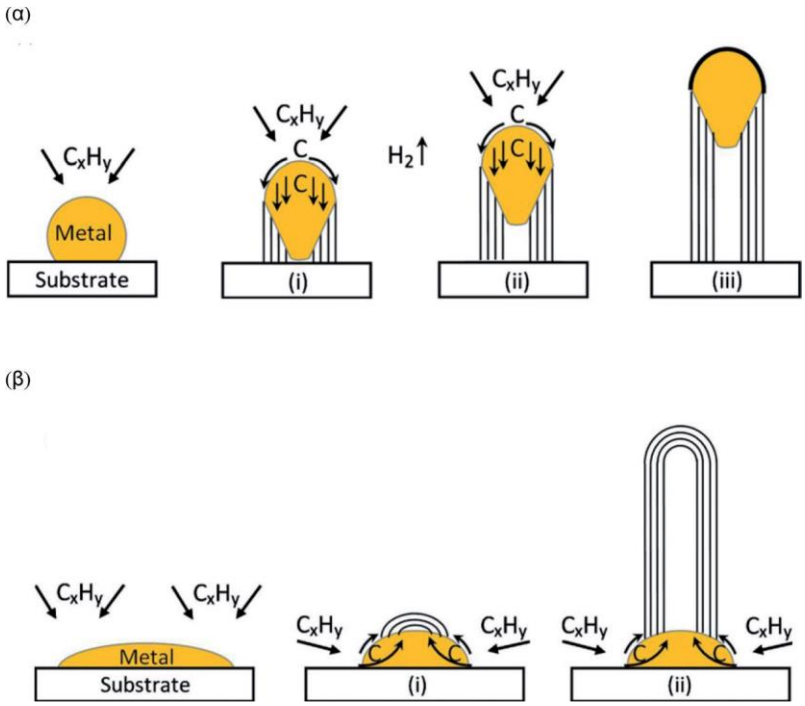

Figure 2-4: Two growth model diagrams for CNTs: (α) tip-growth mechanism (β) root-growth mechanism [26].

The mechanism of CNT growth is comprised of two distinct processes, namely tip growth and root growth (Figure 2-4). Tip-growth is the process by which CNTs grow when metal catalysts interact weakly with the substrate. In this mechanism, carbon derived from hydrocarbons decomposes and diffuses from the metal catalyst to its bottom where it precipitates between the substrate and the catalyst, ultimately promoting the growth of the entire catalyst nanoparticle. This process continues until the metal particle becomes entirely covered by an excess of carbon, which results in growth termination, known as tip-growth. The carbon precipitates from the top of the metal when the catalyst and substrate have a strong interaction, without pushing up the metal particles. This phenomenon is known as the root growth. Regardless of the growth model, whether tip growth or root growth, the catalyst particle is the starting point for CNT growth [26], [27].

2.7 Growth control of CNTs

The growth control of CNTs is a complex process that involves a variety of factors, including the type of catalyst used, the temperature, and the gas environment. Here are some of the key factors that influence the growth of CNTs:

The catalyst used in CNT development is crucial as it influences the CNT type that will be developed. Oxides of transition metals including Fe, Ni, and Co are common catalysts. The catalyst particle's diameter is the most important variable to manipulate for fine-tuning the tube's outer diameter and inner number of layers. The diameter of the synthesized tubes will match the diameter of the catalyst, at least in most cases. Thus, if we regulate the size of the catalyst particles, we can practically adjust the tube's internal dimension. Different catalyst materials may have different properties that affect the CNT growth rate. Some catalysts may promote faster growth, resulting in longer CNTs, while others may result in slower growth and shorter CNTs. The choice of catalyst used to grow CNTs can have an impact on their chirality. This is because the catalyst can influence the growth of the CNT in a specific direction, which determines the angle at which the graphene sheet is rolled up to form the CNT. In other words, the choice of catalyst can influence the growth of the CNTs and determine their chirality. The CNTs' growth rate, diameter, and chirality can all be modified by the type of catalyst used. The synthesis of CNTs relies heavily on the choice of carbon source and carrier gas, as they have a critical impact on the control of tube layer number. The catalyst particle activity can persist for a more extended period, leading to longer tubes when the appropriate carbon source is used. However, if the carbon source is not suitable for the growth conditions, such as furnace temperature and flow rate, then a mix of single, double, and multi-walled nanotubes, as well as deposited amorphous carbons, can be produced. High carbon flow rate can also pose a challenge in synthesizing SWCNTs or DWCNTs, resulting in MWCNTs or significant amorphous carbons. Therefore, using low carbon content carbon sources at the proper feed rate is crucial for efficient synthesis of SWCNTs and DWCNTs. The growth control of CNTs is influenced by both temperature and synthesis time. CNTs are typically grown within a temperature range of 600 ℃ to 1000 ℃, with higher temperatures resulting in faster growth rates, but also an increased likelihood of defects and impurities in the CNT structure. The length of the synthesis time is also a crucial

factor, with longer times leading to larger and more densely packed catalyst particles that can form thicker, closely spaced CNTs, while shorter times result in the opposite. It is important to keep in mind that the ideal synthesis time may vary depending on other factors such as the carbon source, pressure, and growth conditions [27]–[30].

3 Experimental Setup and Procedure

The experimental setup and procedure chapter of this study provides a comprehensive overview of the different stages involved in sample preparation, process parameter selection, and characterization techniques for the growth of CNTs through CVD. A comprehensive understanding of the fundamental principles and a methodical strategy to enhance the growth process are imperative for the successful production of CNTs. The present chapter expounds upon the methodological framework employed in this investigation, comprising the thorough selection of substrate material and catalyst, optimization of parameters for the CVD process, and subsequent characterization of the resultant CNTs. The objective of this chapter is to establish a strong basis for the consistency of the outcomes and promote further progress in the field of CNT research by presenting a comprehensive description of the experimental procedures.

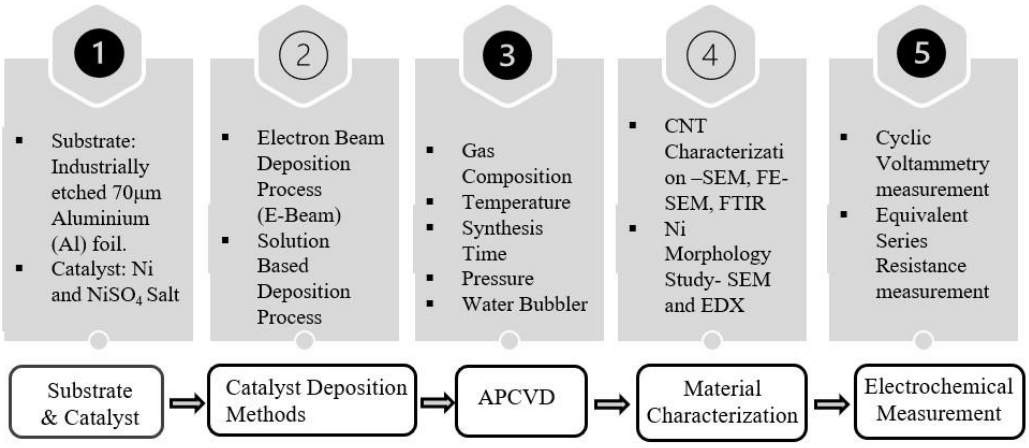

Figure 3-1: Schematic representation of material and methodology study.

3.1 Experimental Setup

3.1.1 Substrate and Catalyst

This study highlights Al as the preferred substrate for iCL-CNT growth optimization process owing to its manifold beneficial characteristics, although not being the exclusive alternative. Al demonstrates superior conductivity in comparison to silver, copper, and gold, thereby facilitating the reduction of the ESR of supercapacitors. Furthermore, the low density and lightweight nature of the material are contributing factors to the

improved energy density and power density measured in supercapacitors. The ductility of Al facilitates the provision of diverse packaging alternatives for supercapacitor architectures, including cylindrical, stacking, or flat jellyroll cells. Diverse chemical and physical techniques, such as acid etching, mechanical lapping, and laser etching, can be employed to produce non-uniform structures on the surface of Al. Moreover, Al demonstrates exceptional chemical stability in the organic electrolytes that are frequently utilized in supercapacitors. The ample presence of this element on the planet enables the creation of economically viable supercapacitors, thereby expanding their availability and cost-effectiveness for diverse applications [24].

The substrate used in this study is an industrially pre-etched Al foil with a thickness of 70 µm provided by FOILTEC (Figure 3-2). The surface of aluminium that has been etched displays increased roughness, thereby facilitating the even distribution of catalyst nanoparticles and strengthening the level of interaction between the catalyst and the substrate. The alteration in the surface chemistry of Al enhances the growth of CNTs, thereby resulting in superior quality CNTs that can be utilized in supercapacitors [24], [31].

Figure 3-2: pre-etched 70µm Al Foil.

This study highlights Ni as the preferred catalyst for the iCL-CNT growth optimization process. The selection of catalysts is of paramount importance in the regulation of CNT production. Nickel-based materials have been recognized as highly efficient catalysts for CNT production due to their remarkable ability to break C-C and C-H bonds. According to

research, the use of smaller nickel nanoparticles, composed of metallic nickel and exhibiting a high degree of distribution on the supporting substrate, plays a significant role in the production of high-quality CNTs. In this study Ni and $NiSO_4$ salt used as catalyst on Al substrate [32].

3.1.2 Catalyst particle (Ni) deposition

The present study employs two separate techniques for loading Ni nanoparticles onto etched Al foil, including electron beam evaporation (E-Beam) and $NiSO_4$ solution-based method using drop and dip coating. The Al foil that has undergone etching is pinned within a vacuum chamber that maintains a pressure range of 5×10^{-7} to 1×10^{-6} Torr. Nickel atoms were simulated through a constant current of 70mA to achieve a deposition rate of 0.04nm/s from a nickel source. Electron beam deposition is conducted at ambient temperature ranging from 20℃ to 25℃, with an argon flow rate of 10-15 standard cubic centimeters per minute(sccm), and under a pressure range of 1×10^{-6} to 5×10^{-6} Torr. Upon removal from the vacuum chamber, the Ni deposited onto the etched Al foil will undergo exposure to the ambient air, leading to the generation of nickel oxide on the Al substrate [24]. These 40nm E-beam samples were provided by a fellow master student from USN.

$$Ni \xrightarrow{Air} NiO_x$$

The preparation of nickel-based solutions can be accomplished by the dissolution of nickel compounds such as Nickel (II) acetate ($Ni(CH_3CO_2)_2$), Nickel(II) nitrate ($Ni(NO_3)_2$), or $NiSO_4$ in ethanol. Subsequently, the Al surface is subjected to drop coating and dip coating with nickel solutions. The single-sided electrode nickel solution is applied exclusively to one side of the etched aluminium foil through drop coating. The deposition of Ni compounds onto the Al substrate is facilitated by the evaporation of the solvent, resulting in a well-coated surface [24]. The dip-coating procedure was initiated by initially introducing the prepared solution into a sterile beaker. The substrates designated for coating were subsequently immersed in the solution. The immersion procedure was repeated four times to achieve a consistent coating on both side of the surface of every samples. Following the conclusion of every dip-coating repetition, samples were subjected to a 5-minute air-drying phase to expedite the ethanol evaporation process. The intermediate drying phase following each immersion cycle played a crucial role in the

settling of the coating, thereby facilitating the uniform distribution of the layer on the underlying surface. The deliberate repetition of the process was strategically devised to amplify the comprehensive coating thickness and consistency.

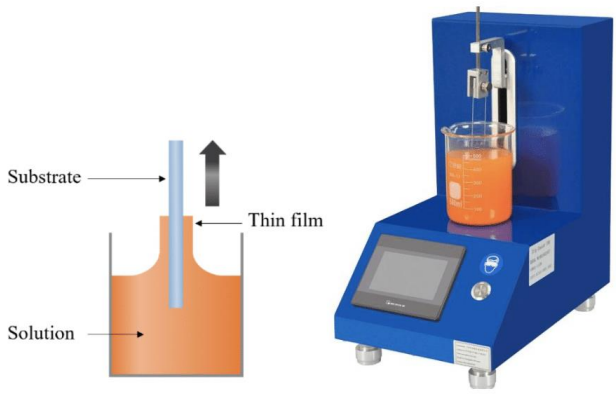

Figure 3-3: Schematic representation of dip coating method [33].

The final thickness of the film in dip coating is dependent on a combination of various factors. Factors that impact the process include the solution's viscosity, the velocity at which the substrate is extracted from the solution, and the gravitational force exerted on the liquid film. Each of these variables is a critical factor in determining the ultimate thickness of the coated film [33].

The drop coating method relies on the interplay between the volume of the dispensed droplet and the concentration of the dispersion to determine film thickness. The size of the droplets and the concentration of the solution are the key variables that govern the process of film formation in this approach. In the context of this study, precise measurement of film thickness is of utmost importance, given its implications on the mass loading of CNTs. After careful evaluation and differentiation of both processes, we have decided to proceed with the drop coating technique. This decision was guided by its greater control over film thickness, facilitated by the adjustable volume and concentration parameters [33].

The present study proceeds solely with a solution of $NiSO_4$ at a concentration of 0.1 M. $NiSO_4$ salt (SIGMA-ALDRICH) was provided by the university. The following equations have described the formation of nickel compounds:

$$NiSO_4 \text{ Solution} \rightarrow NiSO_4.6H_2O$$

$$NiSO_4.6H_2O \xrightarrow{25℃-150℃} NiSO_4+H_2O$$

To measure $NiSO_4$ mass in 0.1M solution following calculation has been followed:

$NiSO_4$ Mass:

$$\frac{0.1 \text{ mol/L} \times 154.7 \text{g/mol (Molar mass of } NiSO_4) \times \text{ethanol(X)mL}}{1000mL}$$

This study employed a 500 mL volume of ethanol and 7.735 g of $NiSO_4$ salt to prepare a solution of 0.1 M $NiSO_4$.The solution was put through an overnight Ultrasonic Bath (FB15051) to ensure proper dilution (5.1).

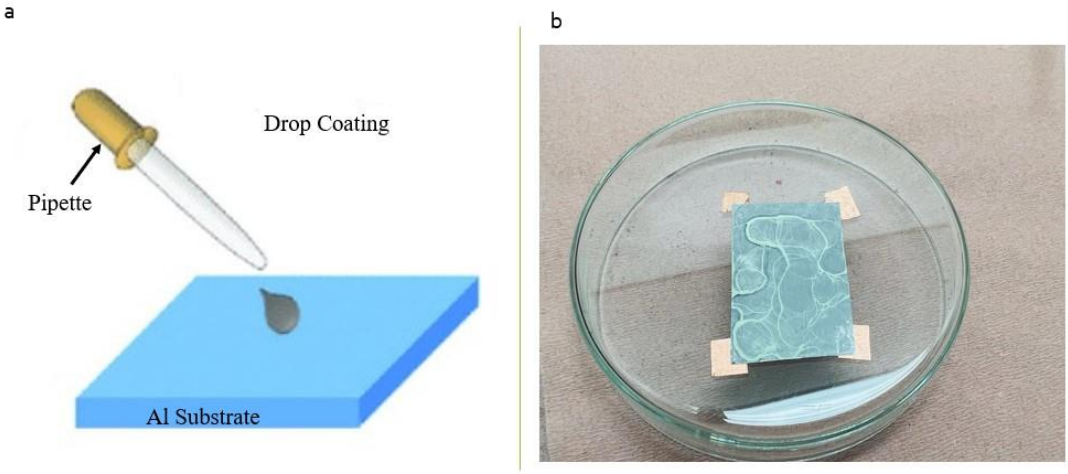

Figure 3-4: (a) Schematic representation of drop coating method (b)Drop coated Sample.

The drop coating technique involves the preparation of Al foil by cutting it to the desired dimensions and afterward cleansing it with ethanol, followed by air-drying. Subsequently, the $NiSO_4$ solution that was previously prepared, along with a petri dish and a sterile

pipette, was placed in a fume hood at ambient temperature to initiate the drop coating technique (*Figure 3-4*). The present investigation employs a quantity of 37.90µl/cm^2 $NiSO^4$ to achieve a thickness of approximately 250nm of Ni layer. Following mathematical calculation has been followed to calculate volume of $NiSO_4$:

Table 3-1: Catalyst layer thickness measurement

Area of the sample (**A**)= 1cm^2 ; Ni thickness(**t**)= 250nm=2.5×10^{-5} cm
Volume of sample $(\boldsymbol{V}) = \boldsymbol{A} \times \boldsymbol{t}$= 2.5×$10^{-5}$ cm^3
Mass of the Ni for the Sample$(\boldsymbol{m}) = \boldsymbol{Density}(\boldsymbol{\rho}) \times \boldsymbol{Volume}\ (\boldsymbol{V})$
Mass of the Ni for the Sample=8.9 g/cm^3 × 2.5×10^{-5} cm^3=22.25×10^{-5} g
100mL solution of 0.1M $NiSO_4$ contains 0.587g Ni.
Required $NiSO_4$ volume for 250nm thickness is = $\frac{22.25\times10-5\ \mathrm{g}}{0.587} \times 100$= 37.90 µL

This is the general formula that has been followed to achieve different thickness of Ni layer thickness. Utilizing a laboratory weighing scale (VWR)(5.2), we calculated the sample's weight prior to drop coating. Then, after the sample has coated with $NiSO_4$, we measured the sample's weight to determine the Ni weight. We need this weight difference to calculate the CNT's mass afterwards.

3.1.3 Morphology study of catalyst particles and CNTs

Analysis using energy-dispersive X-rays (EDX or EDS) has been performed to learn about the morphology of Ni. The EDX method may rapidly yield data regarding the chemical composition of a sample, including the types of elements present and the amounts of those elements. The morphology of Ni has been examined both before and after heat treatment of the drop-coated samples [34].

The characterization of the produced CNTs and Ni particle was conducted through the utilization of both Scanning Electron Microscope (SEM) (Hitachi SU3500) (5.2) and Field Emission Scanning Electron Microscopy (FE-SEM) -Hitachi SU 8230(5.2). Both scanning SEM and FE-SEM can produce high-resolution images of a sample's surface, enabling the observation of the nanoscale structure of CNTs, including their morphology, diameter,

and length. Assessing the quality and uniformity of CNTs holds significant importance in this study.

This study worked with Fourier-transform infrared spectroscopy (FTIR) (5.2) with an excitation source of a 1064nm laser and a maximum power of 0.5W to detect the existence of CNTs and amorphous carbons. The operational principle involves the assessment of the sample's absorption of infrared radiation with respect to the wavelength. The absorption of infrared light at distinct wavelengths by various functional groups and bonds present in the samples generates a distinctive spectrum, which can be employed for the purposes of quantification and identification [35].

The present study applied a three-electrode configuration (Figure 3-8) to quantify the specific capacitance of the electrodes. The setup comprises a reference electrode consisting of silver/silver chloride (Ag/AgCl), a counter electrode that is graphite, and a working electrode composed of grown CNTs. The electrolyte employed in this configuration includes a sodium sulfate (Na_2SO_4) solution with a concentration of 1M. The electrochemical measurements were conducted using a potentiostat (BioLogic VSP-300) (Figure 3-8). The present setup facilitated a thorough evaluation of the capacitive characteristics exhibited by the electrodes constructed using iCL-CNTs in the selected electrochemical setting.

3.2 Procedure

3.2.1 Growth of CNTs and optimization by CVD process

The CNT synthesis system is composed of a quartz process tube that is situated within a horizontal furnace. This furnace is equipped with temperature sensors that are strategically located in three distinct zones, namely the initial, middle, and final sections of the furnace. To carry out each experiment, it is necessary to ensure that several initial conditions are met.

The study's CVD process was initiated through an involved sample preparation procedure. The samples utilized in this investigation exhibited diverse shapes, encompassing circular samples with diameters of 11mm and 18mm, in addition to

rectangular samples measuring (2x3)cm. Every sample was subjected to a thorough cleaning process utilizing ethanol to eliminate any probable contaminants.

Following the cleaning process, the samples underwent a drop-coating methodology. Precise weight measurements were carefully recorded prior to and after the coating procedure to document alterations in mass and, consequently, the degree of coating attained. After the completion of the coating process, the samples were cautiously positioned onto a quartz boat. To ensure the prevention of contamination, the inner tube of the furnace underwent a thorough cleaning process using ethanol before the placement of the sample. To ensure the most favorable heating conditions, the coated samples were placed at the heart of the furnace's heat zone via a quartz boat. The furnace was carefully sealed to prevent any potential air leakage that may disrupt the controlled environment necessary for the CVD process. Upon completion of the necessary arrangements, the heating system of the furnace was initiated and stabilizing the temperature in each heating zone with a tolerance of ± 20℃ (Figure 3-5). Simultaneously, Argon (Ar) gas was purged at a flow rate of 40sccm through a water bubbler that was filled with 500 mL of deionized (DI) water. During the ultimate stage of preparation, the furnace chamber was subjected to evacuation until it attained atmospheric pressure, thereby establishing an optimal environment for the APCVD process.

The present investigation employs Ar as a carrier gas for the purpose of CNT synthesis. This CVD facility consists of gas flow meters to have precise control on each gas flow rate. The synthesis temperature of 600℃ is attained by the furnace within a time span of 58 minutes. It is worth mentioning that most research endeavors that have explored higher mass loading have been carried out under conditions of increased temperature. The structural integrity of the Al substrate must be safeguarded by restricting the maximum temperature to 600℃, as the melting point of the substrate is 660℃.

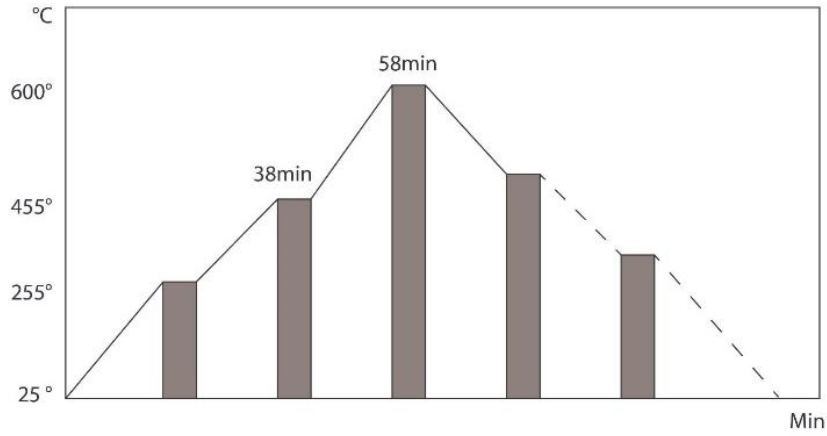

Figure 3-5: Temperature profiling of the furnace.

A flow rate of 100sccm of hydrogen (H_2) gas is introduced into the furnace 20 minutes prior to it attaining a temperature of 600℃. In this phase redox reaction takes place between nickel oxide (NiO) and H_2 to produce metallic nickel.

$$NiO+H_2 \rightarrow Ni+H_2O$$

After attaining the designated temperature, the working chamber is infused with a carbon source in the form of acetylene (C_2H_2) at a rate of 20sccm, while the other gases of Ar and H_2 are sustained. In this phase the following formula takes place to form iCL-CNTs on Al foil.

$$C_2H_2 \xrightarrow{Ni,\&600℃} 2C+H_2$$

The growth of iCL-CNTs was optimized through a series of experiments that involved varying synthesis times and gas compositions. The primary focus of the initial phase of our experimental design was to modulate C_2H_2, which is the primary carbon source in the reaction. This was done by using a total gas flow of 600sccm.

After conducting a series of extensive experiments, have determined the ideal conditions for the simultaneous manipulation of C_2H_2 and Ar. The proportion of the two gases, namely Ar and C_2H_2, has been identified as a crucial factor in regulating the growth of iCL-CNTs.

The present investigation involved subjecting the samples to a pre-heat treatment with 100sccm H_2. This step holds significant importance in the context of solution coating samples, as pre-treatment has the potential to enhance the adhesion between the substrate and the solution coating by prevents the oxidation of the substrate during the heating process and takes place in reduction process as mentioned earlier. This can help to maintain the surface properties of the substrate, promoting better adhesion with the coating. Additionally, it is important that H_2 pre-treatment can exert an influence on the size of the catalyst particles. A set of systematic experiments was carried out to investigate the impact of H_2 flow rate on the growth of CNTs. The present study employed an experimental design that entailed manipulating the H_2 flow rate within a specified range of 5 to 25sccm.

After conducting an analysis of the experimental outcomes, an optimized H_2 flow rate of 100sccm (Figure 3-6) was identified for the growth of CNTs under the specific experimental conditions.

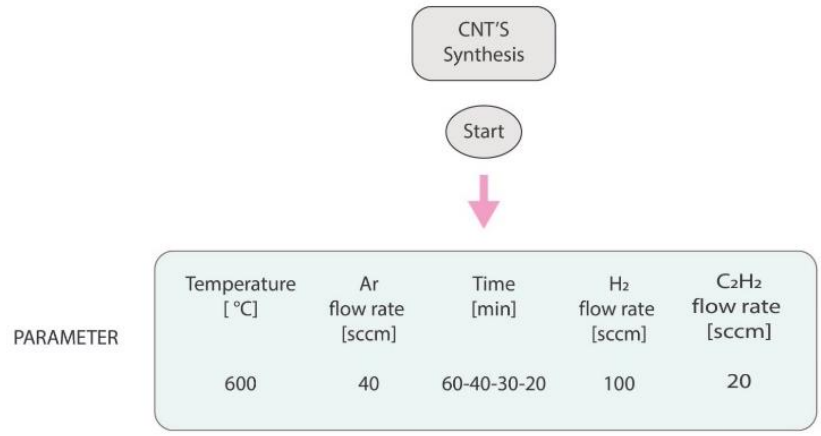

Figure 3-6: Schematic representation of CNT's synthesis parameters.

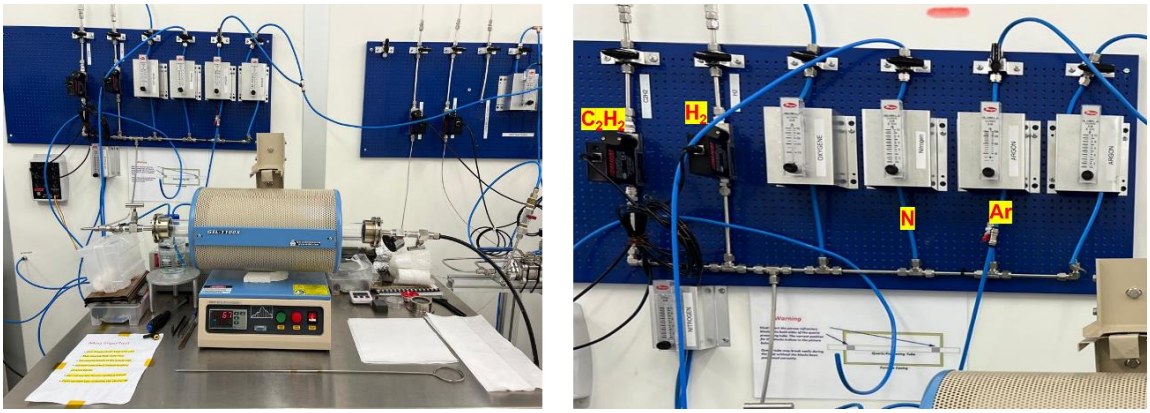

Figure 3-7: (a) APCVD facility (b) gas flow meters of the facility used in this study.

Initial experiments commenced with a synthesis time of 90 minutes. However, upon a comprehensive series of optimization trials, the synthesis duration was significantly reduced. The final optimized synthesis time implemented in the procedure was a particularly shorter duration of 20 minutes. Following the conclusion of the experimental procedures and discontinuation of the supply of C_2H_2, Ar, and H_2, the system is subjected to a purging process utilizing Nitrogen (N_2) at a flow rate of 300sccm for a duration of 2 hours. Subsequently, the furnace is gradually subjected to a cooling process until it reaches a temperature of 25℃, thereby concluding the procedure. Precise extraction of the sample is necessary after the procedure. Upon extraction of the sample, we proceeded to measure the sample's weight to determine the mass loading of grown CNTs. The APCVD machine used in this study is from MTI Corporation model GSL-1100X (Figure 3-7).

3.2.2 Electrochemical measurement

The present study allows for the attainment of iCL-CNTs with a thickness of up to 500 µm~2.8mm and mass loading of approximately ~53mg/cm^2. The adjustment of these parameters is achieved through the control of the volume of the $NiSO_4$ solution and the duration of the synthesis process. The capacitive performance of the iCL-CNTs electrode is investigated through the assembly of a supercapacitor utilizing a 3-electrode setup (Figure 3-8). The counter electrode and electrolyte employed in the experiment consisted of a graphite material and a solution of 1.0M Na_2SO_4. The calculation of the specific capacitance (SC) of the working electrodes was carried out using CV measurements within the potential range of 0 to +0.8V, utilizing the formula as follows:

$$\frac{Area(mA \times V)}{2 \times scan\ rate\left(\frac{mV}{s}\right) \times Area\ of\ the\ working\ electrode(cm^2) \times Potential\ window(V)}$$

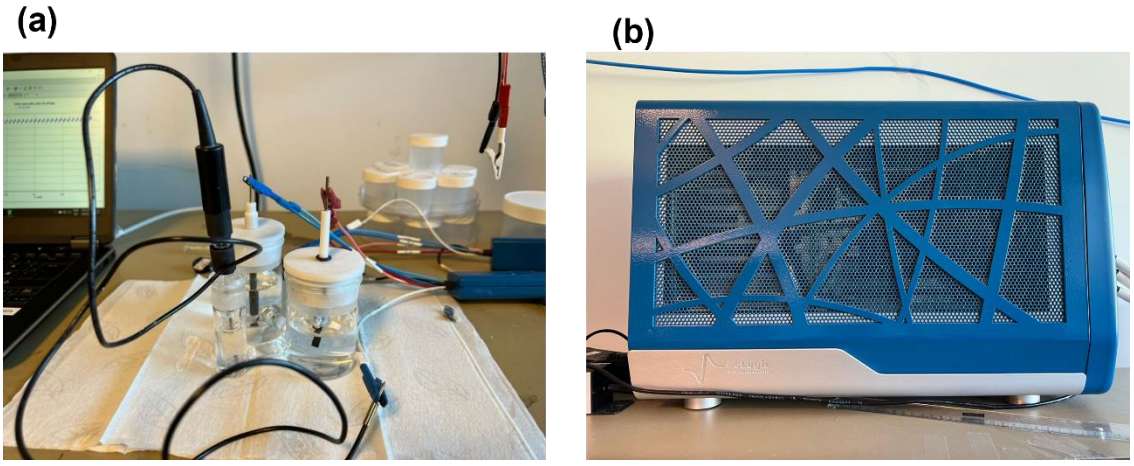

Figure 3-8: (a)3-electrode setup (b) potentiostat.

This study utilized a three-electrode configuration consisting of a working electrode, a reference electrode, and a counter electrode. The working electrode which is iCL-CNTs in this case functions as the central element of the study, wherein it regulates the potential and measures the current. The reference electrode serves as a reliable point of reference for monitoring and regulating the potential within the system, whereas the counter electrode facilitates the closed circuit, thereby enabling electrochemical measurements. The utilization of CV enables precise assessment of electrochemical parameters such as specific capacitance, stability, and ESR in this configuration.

The present study utilized different scan rates, commencing with a rate of 100mV/s to ensure the stabilization of the electrochemical process. Following that, measurements were carried out up to a scan rate of 2mV/s. The mentioned methodology enabled a thorough examination of the electrochemical behaviour and characteristics of the system being studied.

4 Results and Discussion

4.1 Ni morphology study before and after heat treatment

As previously discussed, catalyst particles have a significant impact on the structure and diameter of CNTs. To achieve greater regulation over the growth of CNTs, it is crucial to understand the behavior of catalysts and their chemical state both before and after heat treatment, given that catalyst nanoparticles serve as nucleation centers for CNT growth.

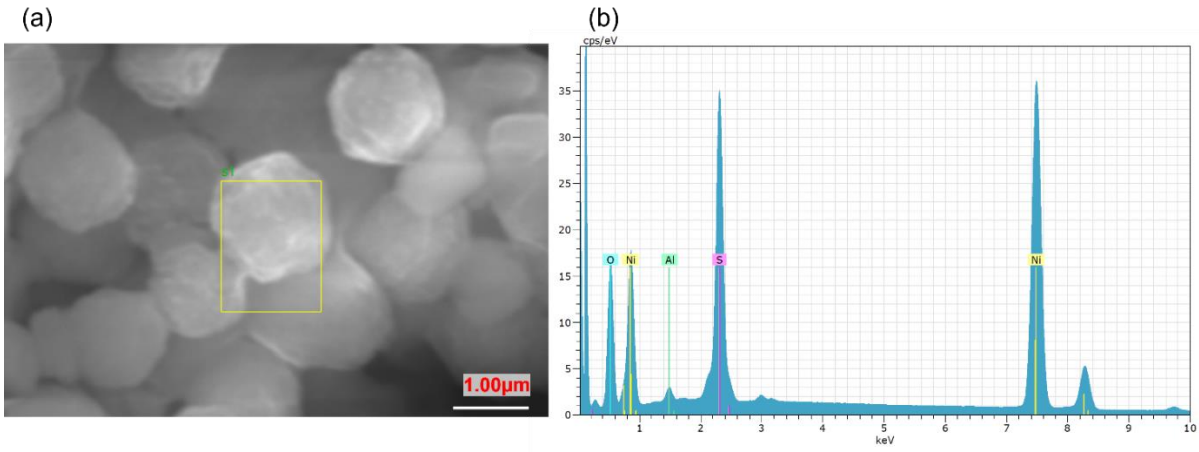

Figure 4-1: Before heat treatment (a)SEM image of $NiSO_4$ cluster (b) EDX result, representing elements present before heat treatment.

Following the $NiSO_4$ drop coating method, a study was conducted to investigate the morphology of $NiSO_4$ before heat treatment. The cluster of $NiSO_4$ represented in (Figure 4-1a) exhibits a polyhedron shape cluster and possesses a surface that is characterized by roughness. The presence of an oxide layer was observed from the strong oxygen peak in the EDX result.

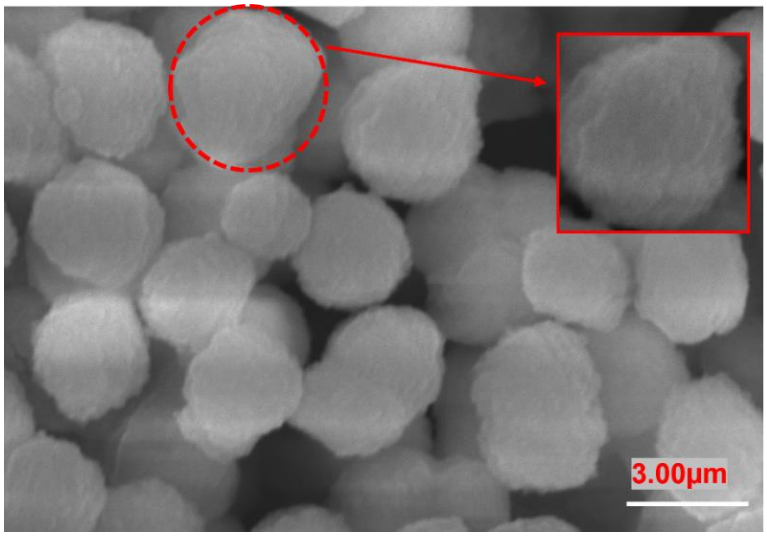

Figure 4-2: $NiSO_4$ cluster before heat treatment.

Upon analysis of (Figure 4-2), it was observed that the $NiSO_4$ clusters exhibited a size distribution ranging from 1.04~1.64µm. The measurements offer significant insight regarding the morphological attributes of the $NiSO_4$ particles before undergoing CVD process. From the EDX results we have observed a similar peak for Sulfur (S) and Ni coupling with oxide layer.

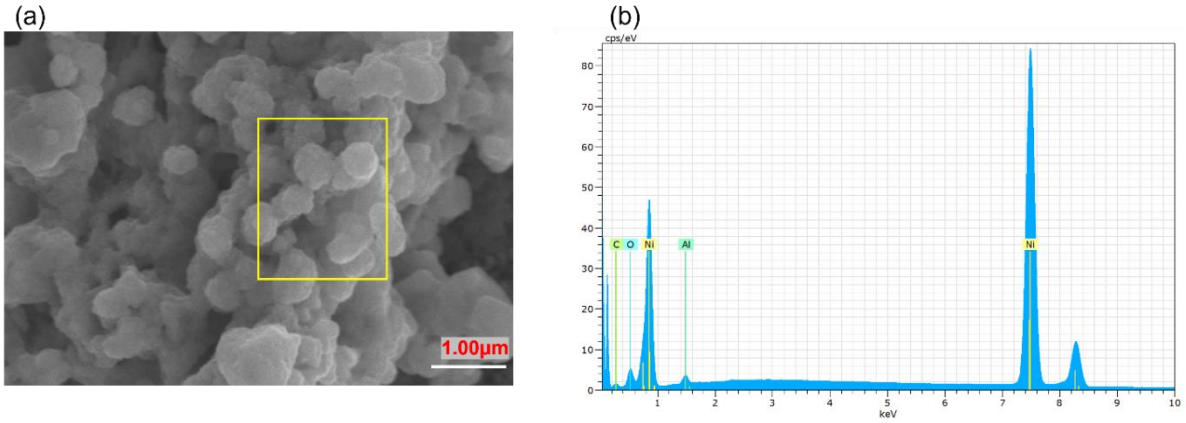

Figure 4-3: After heat treatment (a) SEM image of agglomerated Ni particles (b) EDX result representing the elements present after heat treatment.

Upon undergoing heat treatment in the presence of H_2 gas, $NiSO_4$ decomposes and produces NiO. The NiO then transforms into metallic Ni, assisting in the decomposition of hydrocarbon gases. Following the heat treatment process, there is a phenomenon of Ni particle agglomeration, as illustrated in Figure 4-3(a), which displays the granular structure of these agglomerated Ni particles. The utilization of EDX analysis provided conclusive proof of the transformation of $NiSO_4$ into metallic Ni, which is evidenced by the absence of S peak and weak oxygen peak on Al substrate.

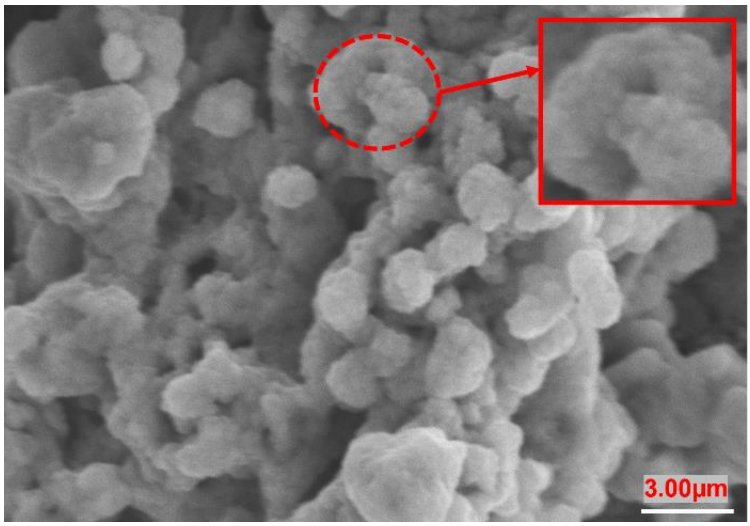

Figure 4-4: Ni particles morphology after heat treatment.

Upon subjecting the sample to heat treatment, a significant reduction in the size of the Ni clusters was observed. Post-treatment measurements indicated that these Ni clusters had decreased to a range of approximately 612~710nm. Moreover, a detailed examination via SEM revealed interesting morphological features of these heat-treated granular shape Ni particles agglomerated clusters. Notably, we identified the presence of smaller Ni particles embedded within the agglomerated Ni clusters.

As previously stated, the diameter of CNTs is primarily influenced by the dimensions of the Ni nanoparticles. Nevertheless, it was not feasible to directly measure the size of single Ni particles in (Figure 4-4) because of the agglomeration but Ni cluster size reduction was observed after heat treatment with H_2. In this study, mathematical calculation (Table 3-1) was used to estimate Ni layer thickness. An etched Al surface may have caused thickness differences from 250nm. FE-SEM was used to analyze drop-coated cross-sectional samples to measure Ni layer thickness. However, the accurate assessment

of the thickness of the Ni layer was inhibited by an excessive quantity of charge accumulation. The study investigated different thicknesses of Ni layers, ranging from 50 to 250nm. The experiment showed mass loadings of up to 40mg/cm^2 for the approximately 250nm thickness of the catalyst layer. Given that one of the keys aims of this study was to attain higher mass loading of CNTs, the following experiments were undertaken to employ an estimated $NiSO_4$ thickness of 250nm.

4.2 Optimization of C_2H_2 and Ar flow

The present study aims to optimize the gas composition by drawing upon existing research on higher mass loading of CNTs in this domain. The study began with a total gas flow of 600sccm [36]. To achieve a higher mass loading of CNTs, a concentration of 3sccm of C_2H_2 was utilized first. The Al substrate was subjected to E-beam deposition to obtain Ni catalyst. The samples were placed within a CVD reactor and subjected to a heating process lasting 58 minutes, followed by a 90-minute hold at 600℃ under an ambient temperature of 497sccm of Ar and 100sccm of H_2 flow rate. Subsequently, C_2H_2 was introduced to initiate CNT growth. In a synthesis period of 90 minutes, approximately 5.2 mg/cm^2 of iCL-CNTs with 38~175nm of diameter were observed to grow on an Al substrate.

Upon increasing the concentration of C_2H_2 to 10sccm, the mass loading correspondingly increased to 10.3mg/cm^2, accompanied by a diameter range of 50 ~163nm of CNTs. This was achieved while maintaining a total gas flow rate of 600sccm. According to the research conducted before [37], the concentration of C_2H_2 increased to 20sccm, resulting in a mass loading of approximately 19.8mg/cm^2 with a diameter ranging from approximately 53 to 180nm(Figure 4-5).

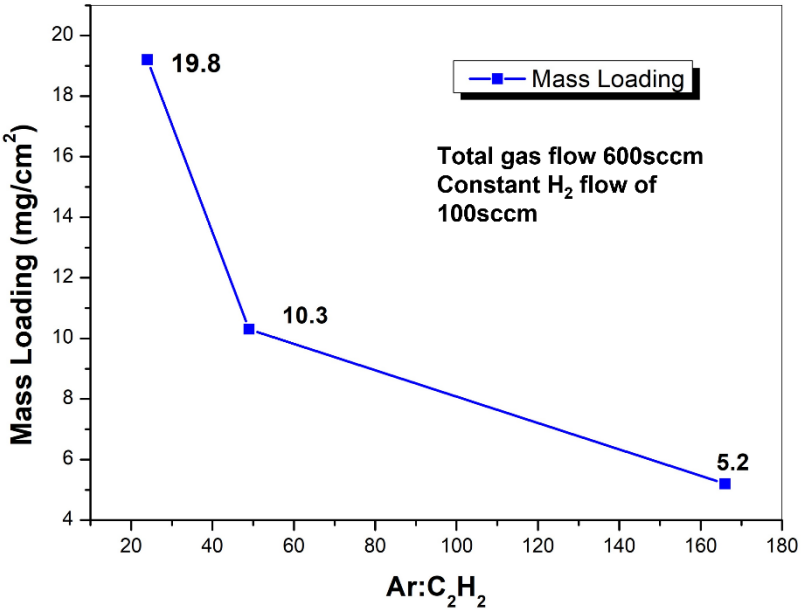

Figure 4-5: Flow rate ratio of Ar:C_2H_2 impact on mass loading of grown CNTs.

This study employed Ar as a carrier gas to transport and dilute reactants, influence gas flow dynamics, regulate temperature, and purge by-products. The carrier gas and hydrocarbon gas ratio must be optimum. Kang Du *et al.* reported a method to grow iCL-CNTs on Al substrate where 50~150sccm Ar was used [24]. The data depicted in Figure 4-5 also illustrates the impact of a lower Ar flow rate on the growth of CNTs, along with C_2H_2. In systematic series of experiments, we lowered the Ar gas flow rate from 300sccm to 40sccm while maintaining a constant synthesis time and temperature and introducing a gas flow of 100sccm H_2 and 20sccm C_2H_2. As a result, we observed an increase in mass loading to 30mg/cm^2 (Table 4-1).

Table 4-1: C_2H_2 and Ar flow rates impact on mass loading of grown CNTs

Gas Ratio (Ar: H_2:C_2H_2) (sccm)	CNT Mass Loading of 40nm (E-Beam) Samples (mg/cm^2)	Synthesis time (min)	Temperature (^{0}C)
497(W): 100:3	5.2	90	600
490(W): 100:10	10.3	90	600
480(W): 100:20	19.8	90	600
300(W): 100:20	22.2	90	600
40(W): 100:20	30.1	90	600

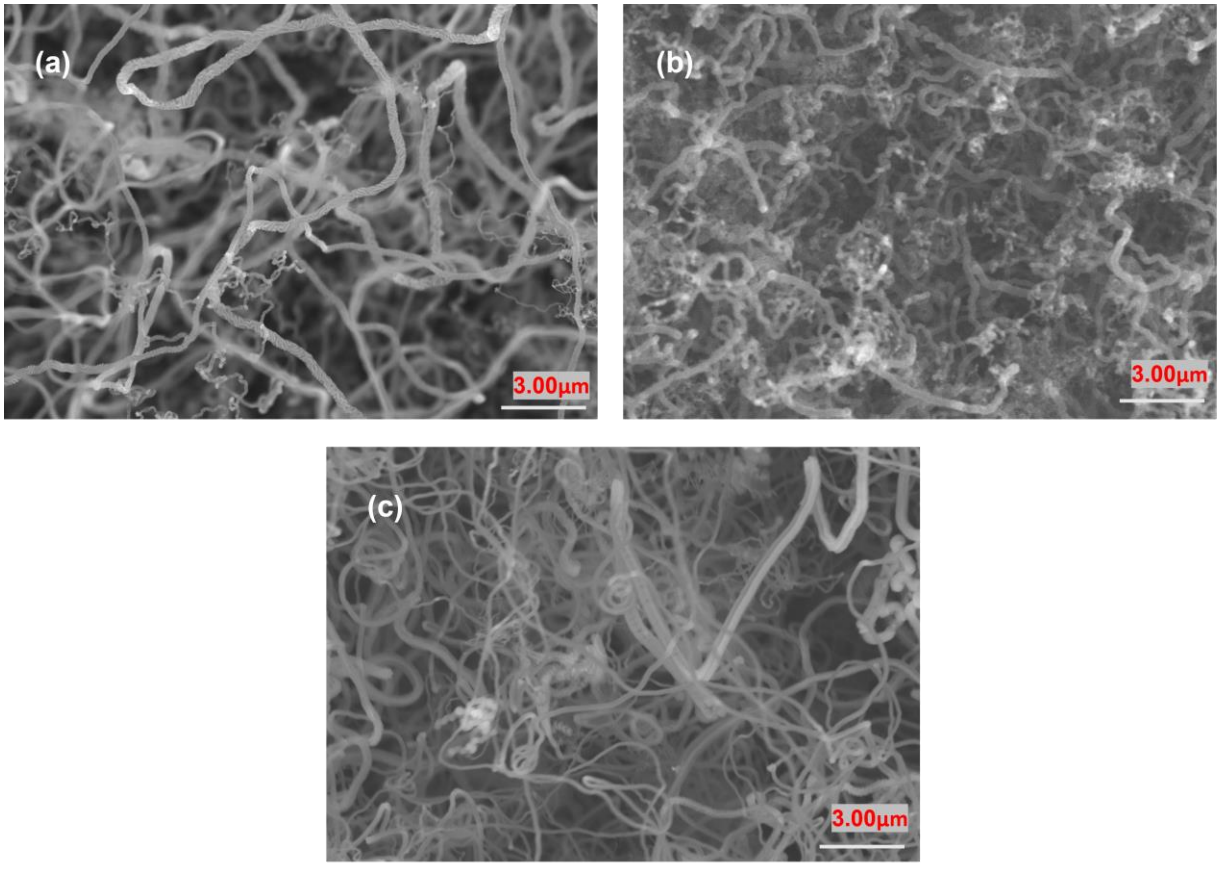

Figure 4-6: Morphology of CNTs grown for flow rate of C_2H_2 (a)3sccm (b)10sccm (c)20sccm.

When the flow rate was increased to 20sccm of C_2H_2 relative effects were seen in mass loading, comparatively long and cross-linked CNTs were observed as compared

to 3sccm and 10sccm flow rate(Figure 4-6), where diameter of CNTs lies in the approximately same range of 40~190nm [37]. The growth rate of CNTs is almost linearly proportional to the C_2H_2 concentration which is also observed in increase mass loading from 5.2 to 30.1mg/cm^2 (Table 4-1). Low C_2H_2 concentrations may not provide enough carbon atoms for CNT growth. This can lead to a lower mass loading of CNTs and a slower growth rate. We have observed the same scenario while using 3sccm of C_2H_2. The C_2H_2 gas flux also determines the number of carbon atoms available in the reactor for the growth of CNTs. A higher hydrocarbon gas flux can provide a larger number of carbon atoms, leading to faster CNT growth and higher mass loading [38]. In this study, it was found that a flow rate of 20sccm for C_2H_2 resulted in a higher flux, which subsequently led to an increased mass loading of CNTs.

flux of C_2H_2 for 3sccm=0.21mL/min/cm^2

flux of C_2H_2 for 10sccm=0.68mL/min/cm^2

flux of C_2H_2 for 20sccm=1.37mL/min/cm^2

The findings of the study reported by Toussi *et al.* indicate that a high flow rate of Ar carrier gas resulted in the majority of the carbon source being carried out through the reactor outlet, thereby preventing its deposition on the catalyst. Consequently, only a small amount of CNTs were formed [39]. In this study, we investigated the effect of varying the flow rate of the carrier gas, Ar, while maintaining a constant C_2H_2 flow rate of 20sccm and H_2 100sccm. It was observed that when the Ar flow rate was reduced, the mass loading also increased to 30mg/cm^2 (Figure 4-7).

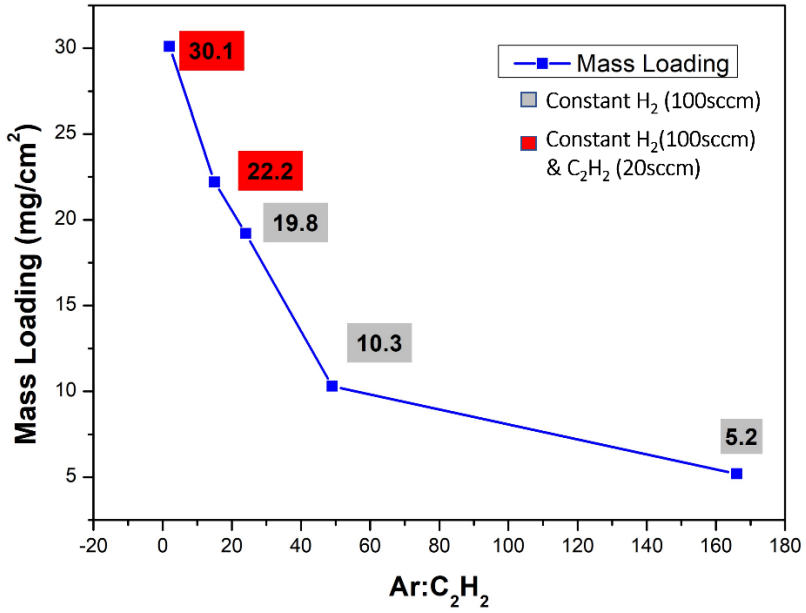

Figure 4-7: Ar flow rates impact on mass loading of CNTs.

Based on the experimental results, the optimal flow rate for the carrier gas was determined to be 40sccm. At this flow rate, the Ar gas effectively transports the required amount of carbon source (20sccm of C_2H_2) into the reactor. Furthermore, this flow rate allows sufficient time for the carbon source to decompose and deposit on the catalyst, facilitating CNT growth.

In this study, the Ar gas was passed through a water bubbler to enhance the catalytic activity during CNT growth via CVD process. The introduction of water vapor, a weak oxidizer, in conjunction with the carbon source has been shown to improve catalyst performance. This optimized combination of carrier gas flow rate and the presence of water vapor demonstrates the importance of carefully controlling process parameters to achieve efficient CNT growth using the CVD method [40].

4.3 Effects of H_2 gas on CNT growth

The growth of CNTs during CVD is significantly influenced by H_2. The growth process of CNTs can be influenced by H_2 through various mechanisms. The activation of catalysts involves the utilization of hydrogen gas as a reducing agent during the CVD process. This

process facilitates the reduction of metal oxide catalyst precursors to their metallic states. The presence of the metallic configuration of the catalyst is a prerequisite for the initiation of CNT growth. Moreover, H_2 has the potential to eliminate any oxide layer that may have formed on the surface of the catalyst, thereby preserving the activity of the catalyst.

The process of CNT growth can result in the formation of amorphous carbon or disordered carbon as a by-product, in addition to the intended nanotube structures. Consequently, the elimination of amorphous or disordered carbon is necessary. The selective removal of amorphous or disordered carbon through the presence of H_2 can enhance the purity and quality of the resultant CNTs, while leaving the CNT structures unaffected. Through precise control of the hydrogen gas flow rate, it is possible to optimize the growth parameters to yield good quality CNTs possessing specific properties [41]. Wen *et al.* claimed that there is a relationship between the catalyst particles with H_2 pretreatment and CNTs growth, as low density of CNT occurs with no H_2 pretreatment. An optimal amount of H_2 pretreatment was also noted as too long a treatment started to decrease the yield of CNTs [42].In this study 20 min H_2 pretreatment was introduced along with Ar through water bubbler. In this inquiry we have investigated the impact of H_2 on mass loading by varying its flow rate from 5sccm to 25sccm (Figure 4-8)

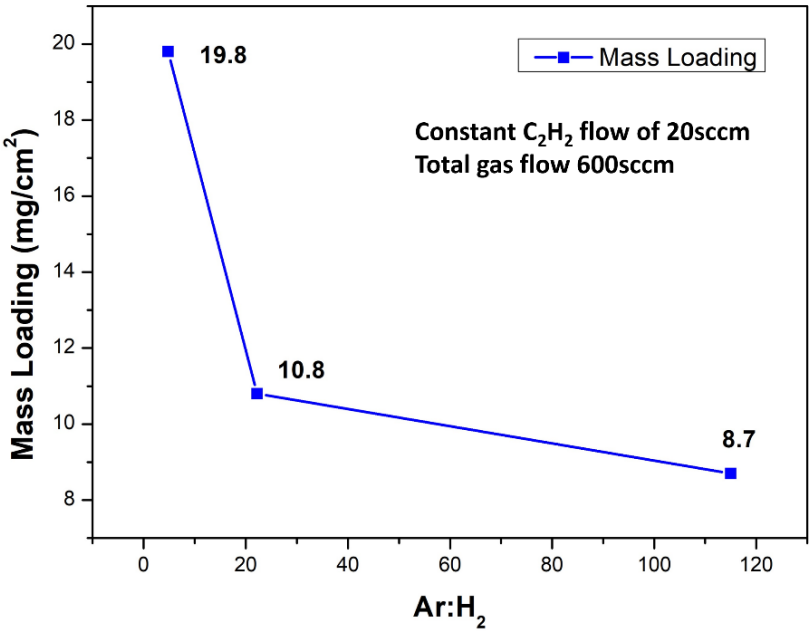

Figure 4-8: Mass loading of CNTs at different H_2 flow rate.

Table 4-2: H_2 flow rates impact on mass loading of CNTs

Gas Ratio (Ar: H_2:C_2H_2) (sccm)	CNT Mass Loading of 40nm (E-Beam) Samples (mg/cm^2)	Synthesis time (min)	Temperature (^{0}C)
575(W): 5:20	8.7	90	600
555(W): 25:20	10.8	90	600
480(W): 100:20	19.8	90	600
300(W): 100:20	22.2	90	600
40(W): 100:20	30.1	90	600

The findings of the experiment, as depicted in Table 4-2, suggest that lowered mass loadings of CNTs were observed in instances where 5sccm and 25sccm H_2 flow rates were employed, as compared to the utilization of 100sccm H_2 flow rate. The ineffectiveness in converting the metal oxide catalyst (NiO) to its metallic state can be defined as the insufficient quantity of H_2 present at flow rates of 5sccm and 25sccm. Insufficient H_2 concentration may not serve to sustain the catalyst's activity, thereby resulting in a reduction in the mass loading of CNTs (Figure 4-8) These findings emphasize the

importance of optimizing the H_2 flow rate to ensure effective catalyst activation and efficient CNT growth.

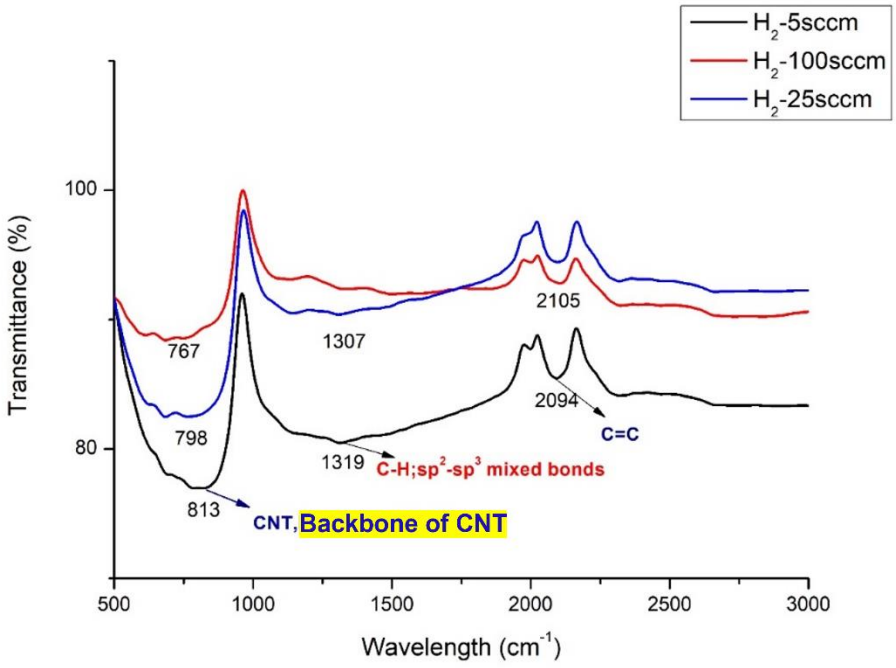

Figure 4-9: FTIR spectra for CNTs and amorphous carbon; at different flow rate of H_2.

As stated earlier, low concentration of H_2 can lead to amorphous or disordered carbon. Figure 4-9 FTIR spectra represents the band from 1300-1515cm^{-1} corresponding to C-H from sp^2-sp^3 mixed bonds (amorphous carbon). The curve (for 5sccm H_2) 1319 cm^{-1} corresponds to low transmittance means there is a high number of bonds present that have vibrational energies corresponding to the incident light [43]. Therefore, it can be said that there were amorphous carbons present while using lower concentration of H_2. The band from 500-1000cm^{-1} corresponds to CNTs, backbone of CNT.

4.4 Synthesis time optimization

Following the optimization of the gas ratio iCL-CNTs growth on E-beam deposited samples, we proceeded to investigate $NiSO_4$ drop-coated samples as an alternative. Additionally, the solution coating method presents a more cost-effective option in

comparison to the E-beam deposition technique. For the drop-coated samples, we observed a mass loading of 36.5mg/cm^2 of CNTs when employing the optimized gas composition for a same synthesis duration of 90minutes at a temperature of 600℃. However, despite the increased mass loading, the adhesion of the CNTs did not exhibit significant improvement. According to the study, when the synthesis time exceeds 60 minutes, an increased amount of disordered carbon is deposited. This is explained by the absence of active catalyst sites and the continuous decomposition of the remaining carbon particles [44] and this may lead to weak adhesion of CNTs. In this study, a reduction in the synthesis time to 60minutes resulted in a mass loading of 53mg/cm^2 with a film thickness of 2.8mm (Figure 4-10). However, there was limited enhancement in the adhesiveness of CNTs.

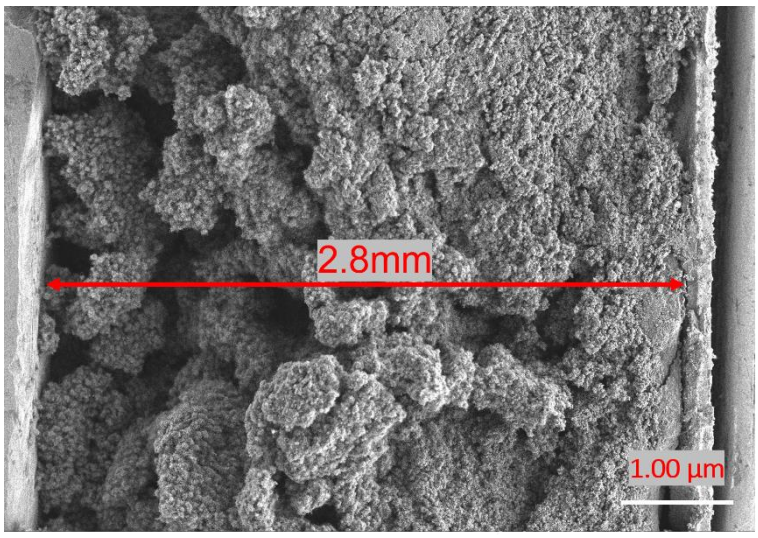

Figure 4-10: FE-SEM image of 2.8mm film thickness of 53mg/cm^2 mass loading of CNTs.

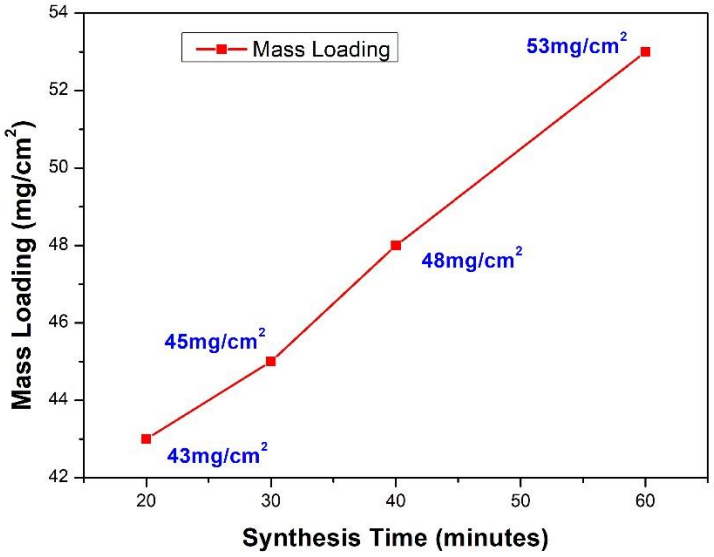

Figure 4-11: Synthesis times impact on mass loading.

Through a series of systematic experiments, it was observed that the synthesis time lowered from 60minutes to 20minutes at a temperature of 600℃, with a mass loading range from 53mg/cm^2 to 43mg/cm^2 (Figure 4-11) and a diameter range of approximately 50~150nm (Figure 4-12).

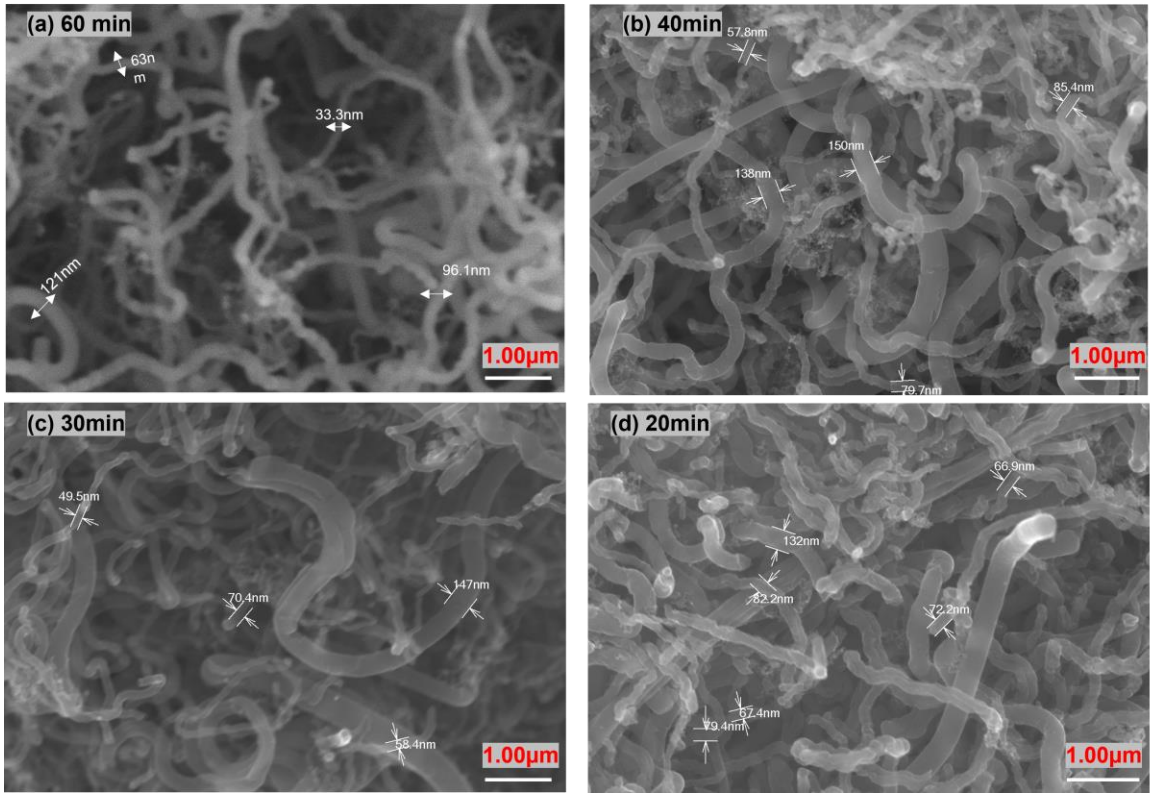

Figure 4-12: (a) for 60 min ⌀-50~150nm (b) for 40 min ⌀-57.8~150nm (c) for 30min ⌀-49.5~147nm (d) for 20 min ⌀-63.4~132nm.

As the duration of synthesis was reduced from 60minutes to 20minutes, there was an observed enhancement in adhesiveness of the grown CNTs. Therefore, a synthesis time of 20 minutes was determined to be the optimal duration for completing the bond-breaking process between carbon and hydrogen atoms during the synthesis procedure. Following that, the CNTs were fully deposited onto the Al substrates, whereby the carbon underwent complete decomposition, diffusion, and condensation to yield a nanotubular architecture.

Table 4-3: Specific capacitance and ESR measurements for different synthesis time

Synthesis Time (min)	CNT Mass Loading (mg/cm^2)	Areal Capacitance(mF/cm^2) at Scan rate 2mV/s	Gravimetric Capacitance (F/g)	ESR(Ω)
60	53	928	17.51	4.84
40	48	1391	28.98	4.23
20	43	1486	34.56	3.08

A series of systematic experiments were conducted to observe the effects of reduced synthesis time on the specific capacitance and ESR calculation. The results, as presented in Table 4-3, indicate a reduction in synthesis time from 60minutes to 20minutes has an impact on specific capacitance, mass loading and ESR as well. The results of the capacitance calculation indicate that a synthesis time of 20minutes leads to a higher specific capacitance and a lower ESR value. An increase in mass loading leads to a decrease in capacitance and an increase in ESR due to the densification of the electrode, which impedes the electrolyte's ability to penetrate and interact with the active material. Insufficient penetration of electrolytes leads to reduced utilization of the active material of the electrode, thereby causing a drop in capacitance and with $53mg/cm^2$ mass loading same scenario was observed [45].

The increase of mass loading results in the elongation of diffusion pathways for ions present in the electrode material, which consequently causes a slowdown in the rates of ion diffusion. The above-mentioned phenomenon can have an adverse effect on the electrode's rate capability, leading to an overall reduction in its capacitance. Nevertheless, the process of assembling coin cell and 3-electrode measurement becomes challenging due to such high mass loading.

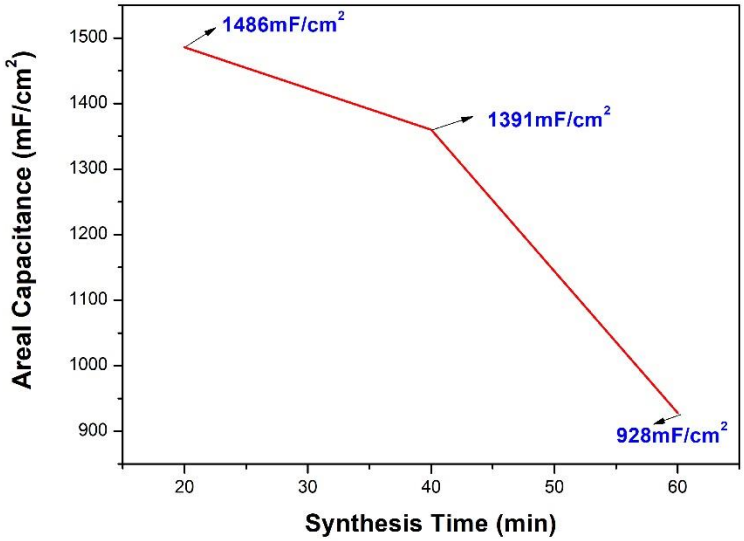

Figure 4-13: Synthesis times impact on areal capacitance.

Also reducing the synthesis time may lead to enhanced adhesion by limiting the growth of thicker and densely packed CNTs, which are more liable for detachment of the CNT's layers from the substrate. Enhancement in adhesion of CNTs lead to higher capacitance as well which was also observed in Figure 4-13 as reducing the synthesis time leading better adhesiveness which resulting higher capacitance. The current study shows that capacitance enhancement is also dependent upon the optimal mass loading because of the phenomena mentioned above. To regulate the mass loading, the most effective approach is to regulate the volume of the $NiSO_4$ solution.

Table 4-4: Mass loading of CNTs for different $NiSO_4$ volume

Volume of $NiSO_4$ Solution($\mu L/cm^2$)	CNT Mass Loading (mg/cm^2)	Areal Capacitance (mF/cm^2)
38.5	45.1	1580
50% reduction in Volume	40.2	1212
70% reduction in Volume	32.5	1181

The experimental results represented in Table 4-4 were obtained following a 20minute synthesis period at a temperature of 600℃. Hence, it can be suggested that regulating the volume of $NiSO_4$ is a systematic way to control mass loading in contrast to the duration of synthesis.

4.5 Comparison of water-assisted CVD and non-water-assisted CVD

The enhancement of CNTs growth through CVD was discovered by Hata *et al.* in 2004 [46]. This was achieved by introducing small amounts of water alongside the carbon source. It is suggested that the presence of water can effectively prolong the lifespan of a catalyst through the process of etching the amorphous carbon accumulation on its surface. According to reference [47], when exposed to ideal growth conditions, a proportion exceeding 85% of the catalyst nanoparticles exhibit activity. The growth kinetics exhibit significant extension, as evidenced by the rapid growth of vertically aligned CNTs film thickness reaching millimeter heights within a few minutes [48]. Thus, the technique involving the use of water in the CVD process has been designated as the "Super growth CVD process" [40].

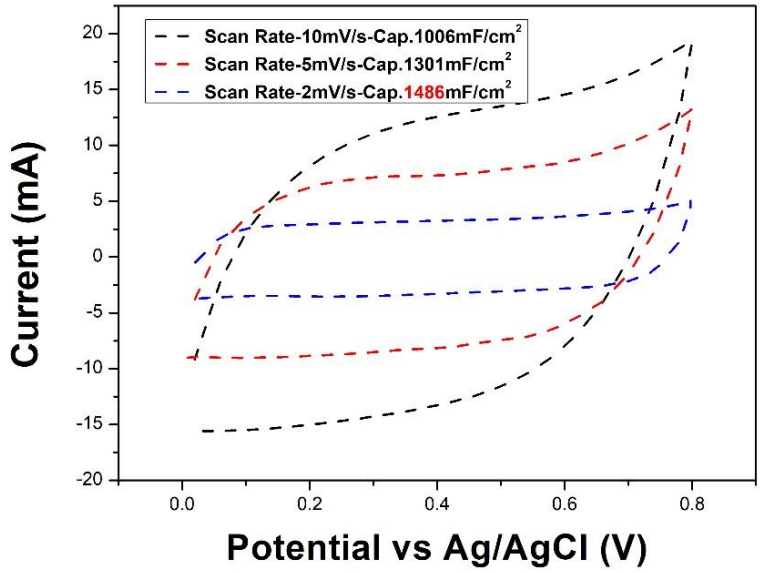

Figure 4-14: Areal capacitance at different scan rates for grown CNTs using water-assisted CVD.

In this study, a water-assisted CVD process was initially employed under optimized growth conditions and observed millimeter height iCL-CNTs along with areal capacitance of 1486mF/cm^2(Figure 4-14).

To further investigate the effects of water on the CVD process, a comparative study was conducted utilizing the same optimized gas composition and synthesis duration in the absence of water. The iCL-CNTs synthesized through the CVD process displayed similar adhesion and slightly increased mass loading in the absence of water.

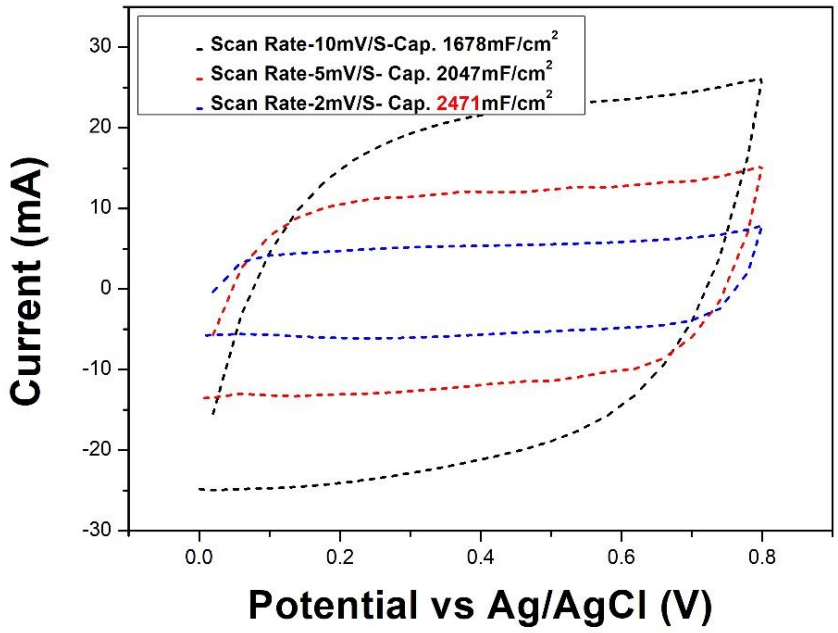

Figure 4-15: Areal capacitance at different scan rates for grown CNTs using non-water-assisted CVD.

However, they exhibited a significantly improved areal capacitance of 2471mF/cm^2 (Figure 4-15). To provide additional clarification regarding the morphological characteristics of these CNTs, a comprehensive examination of the SEM images was carried out (Figure 4-16).

Table 4-5: Comparison between water assisted-CVD and non-water assisted-CVD.

Parameters	Water-Assisted CVD	Non-Water-Assisted CVD
Ar: H_2:C_2H_2 (sccm)	40 :100: 20	40 :100: 20
Temperature (℃)	600	600
Synthesis Time (min)	20	20
Mass Loading (mg/cm^2)	43	46.5
Film thickness (mm)	1.1	1.45
Areal Capacitance (mF/cm^2)	1486	2471
Gravimetric Capacitance(F/g)	34.56	53.14
ESR (Ω)	3.09	3.87

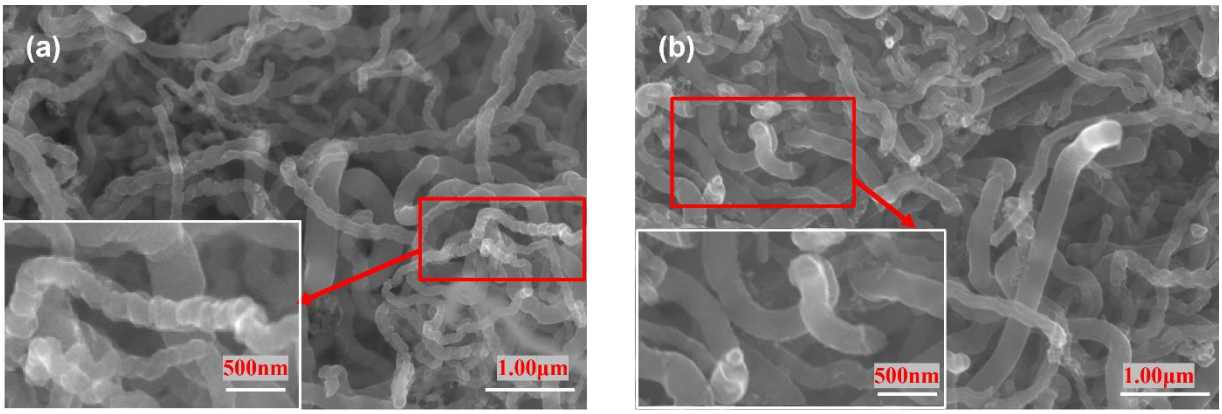

Figure 4-16: Morphology study of CNTs (a)non-water-assisted CVD (b)water-assisted CVD.

A study was conducted to investigate the rapid growth of 1mm vertically aligned small-diameter VA-MWNTs through the utilization of APCVD without water assisted [36]. In this study similar rapid growth of approximately 1.45mm thickness of iCL-CNTs film were observed with significantly improved areal and gravimetric capacitance. Without water assisted CVD process can lead to impurities and defects in CNTs. The study reveals that CNTs possessing defective outer walls exhibit an enhanced capacitance. Additionally, the presence of a thin amorphous carbon layer on the CNTs' surfaces contributes to improved charge accumulation, further highlighting the significance of these structural modifications in the electrochemical performance of the CNTs [49]. From SEM characterization (Figure 4-16), have observed some defects or impurities on CNT's wall as well. These defects or impurities may lead to this 2471mF/cm^2 areal capacitance and 53.14F/g gravimetric capacitance in this investigation. From the comparison Table 4-5 it's clear that non-water-assisted CVD leads to higher mass loading compared to water-assisted and this mass loading difference may lead this higher capacitance as well. But similar mass loading was also observed in water-assisted CVD which didn't exhibit such high capacitance. Coupling with higher mass loading these defects or impurities may be the possible reasoning for higher capacitance.

5 Conclusion and Future Scope

The present study focuses on examining the synthesis of iCL-CNTs on Al substrates. The study revealed that C_2H_2 demonstrated significant effectiveness as a carbon source for the growth of CNTs at a temperature of 600℃. The process necessitated a concentration of 20sccm C_2H_2 at atmospheric pressure, coupled with 40sccm of Ar and 100sccm of H_2 to sustain the activity of Ni particles. While extended synthesis durations led to increased mass loading, the adhesiveness of CNTs did not exhibit improvement due to the negative impacts of prolonged growth periods on CNT's adhesion. Prolonged durations can lead to the development of CNT's film thickness that are thick or densely packed, rendering them vulnerable to mechanical breakdown due to Van der Waals forces, thereby increasing their likelihood of detachment from the Al substrate. Extended periods of synthesis may result in adverse effects on the adhesion of CNTs due to catalyst deactivation, agglomeration, or excessive oxidation. Through the implementation of various synthesis durations, it has been determined that a synthesis time of 20minutes is the optimal duration. This duration yields a high mass loading, improved adhesiveness, and increased specific capacitance.

The results of a set of systematic experiments indicated that the mass loading was subject to variation based on the duration of the synthesis process. However, this methodology did not provide precise regulation of mass loading due to its influence on catalyst activation and additional parameters. In contrast, the present study revealed that the alteration of $NiSO_4$ volume imposed a direct impact on mass loading and mass loading has direct influence on capacitance.

CNTs exhibit remarkable growth through the utilization of water-assisted CVD methodology. The inclusion of a consistent quantity of water vapor during the process results in the formation of CNTs with improved morphology. This study has revealed a significant finding that the super growth of CNTs exhibiting improved adhesion and higher areal capacitance 2471mF/cm^2 can be attained without the aid of water. The synthesis process was carried out for a duration of 20minutes without the aid of water. The proposed hypothesis for achieving super growth with non-water-assisted CVD

suggests that, when employing shorter synthesis times, a suitable concentration of H_2 sustains catalyst activity. Additionally, the elimination of amorphous carbon by H_2 that has accumulated on the catalyst particle surface is believed to improve growth, similar to the function of water vapor. The investigation of the morphology of synthesized CNTs in the absence of water has indicated the existence of defective structures that may result in increased capacitance. Prospective possibilities for research entail additional investigation into the superlative growth of CNTs in the absence of water, as well as the defective structures that appear in CNT's morphology study.

The study did not yield conclusive evidence regarding the correlation between catalyst diameter and CNT's diameter, and the precise measurement of catalyst layer thickness was not attained. The diameter of the CNTs that were grown and observed in both E-beam and drop-coated samples exhibited a range of approximately 50nm to 180nm. To get better understanding and control the diameter and growth of iCL-CNTs, further comprehensive analyses of catalyst Ni particles, their diameters and layer thickness are imperative. Furthermore, given the limited research on the use of $NiSO_4$ for catalyst layer, further exploration of $NiSO_4$ as a catalyst option is a promising avenue for future studies.

References

[1] K. Naoi, W. Naoi, S. Aoyagi, J. Miyamoto, and T. Kamino, "New Generation 'Nanohybrid Supercapacitor,'" *Acc. Chem. Res.*, vol. 46, no. 5, pp. 1075–1083, May 2013, doi: 10.1021/ar200308h.

[2] M. Gidwani, A. Bhagwani, and N. Rohra, "Supercapacitors: the near Future of Batteries".

[3] M. Winter and R. J. Brodd, "What Are Batteries, Fuel Cells, and Supercapacitors?," *Chem. Rev.*, vol. 104, no. 10, pp. 4245–4270, Oct. 2004, doi: 10.1021/cr020730k.

[4] R. A. Fisher, M. R. Watt, and W. Jud Ready, "Functionalized Carbon Nanotube Supercapacitor Electrodes: A Review on Pseudocapacitive Materials," *ECS J. Solid State Sci. Technol.*, vol. 2, no. 10, pp. M3170–M3177, 2013, doi: 10.1149/2.017310jss.

[5] E. Frackowiak, K. Metenier, V. Bertagna, and F. Beguin, "Supercapacitor electrodes from multiwalled carbon nanotubes," *Appl. Phys. Lett.*, vol. 77, no. 15, pp. 2421–2423, Oct. 2000, doi: 10.1063/1.1290146.

[6] J. M. Baptista, J. S. Sagu, U. W. Kg, and K. Lobato, "State-of-the-art materials for high power and high energy supercapacitors: Performance metrics and obstacles for the transition from lab to industrial scale – A critical approach," *Chem. Eng. J.*, vol. 374, pp. 1153–1179, Oct. 2019, doi: 10.1016/j.cej.2019.05.207.

[7] Department of Electrical and Electronics Engineering, SRM University, Kattankulathur, India 603203. and Z. S. Iro, "A Brief Review on Electrode Materials for Supercapacitor," *Int. J. Electrochem. Sci.*, pp. 10628–10643, Dec. 2016, doi: 10.20964/2016.12.50.

[8] L. James, "Supercapacitor: Workings and applications," Apr. 24, 2020. https://www.power-and-beyond.com/supercapacitor-workings-and-applications-a-9dd11c509fefd4ca7e2db6e586e445cf/ (accessed Apr. 27, 2023).

[9] "Electrochemical Capacitor - an overview | ScienceDirect Topics." https://www.sciencedirect.com/topics/engineering/electrochemical-capacitor (accessed Apr. 27, 2023).

[10] E. Frackowiak, "Carbon materials for supercapacitor application," *Phys. Chem. Chem. Phys.*, vol. 9, no. 15, p. 1774, 2007, doi: 10.1039/b618139m.

[11] S. I. Cha, K. T. Kim, K. H. Lee, C. B. Mo, Y. J. Jeong, and S. H. Hong, "Mechanical and electrical properties of cross-linked carbon nanotubes," *Carbon*, vol. 46, no. 3, pp. 482–488, Mar. 2008, doi: 10.1016/j.carbon.2007.12.023.

[12] T. Chen and L. Dai, "Carbon nanomaterials for high-performance supercapacitors," *Mater. Today*, vol. 16, no. 7–8, pp. 272–280, Jul. 2013, doi: 10.1016/j.mattod.2013.07.002.

[13] S. lijima, "Helical microtubules of graphitic carbon," Oct. 1991.

[14] A. Aqel, K. M. M. A. El-Nour, R. A. A. Ammar, and A. Al-Warthan, "Carbon nanotubes, science and technology part (I) structure, synthesis and characterisation," *Arab. J. Chem.*, vol. 5, no. 1, pp. 1–23, Jan. 2012, doi: 10.1016/j.arabjc.2010.08.022.

[15] S. lljima and T. lchihashi, "Single-shell carbon nanotubes of 1-nm diameter," Jun. 1993.

[16] A. Eatemadi *et al.*, "Carbon nanotubes: properties, synthesis, purification, and medical applications," *Nanoscale Res. Lett.*, vol. 9, no. 1, p. 393, Dec. 2014, doi: 10.1186/1556-276X-9-393.

[17] G. D. Nessim, “Properties, synthesis, and growth mechanisms of carbon nanotubes with special focus on thermal chemical vapor deposition,” *Nanoscale*, vol. 2, no. 8, p. 1306, 2010, doi: 10.1039/b9nr00427k.
[18] R. H. Baughman, A. A. Zakhidov, and W. A. de Heer, “Carbon Nanotubes: The Route toward Applications,” *Sci. New Ser.*, vol. 297, no. 5582, pp. 787–792, 2002.
[19] Y. Gao *et al.*, “Direct Intertube Cross-Linking of Carbon Nanotubes at Room Temperature,” *Nano Lett.*, vol. 16, no. 10, pp. 6541–6547, Oct. 2016, doi: 10.1021/acs.nanolett.6b03184.
[20] “Schematic representation of chemical vapor deposition (CVD) process. a...,” *ResearchGate*. https://www.researchgate.net/figure/Schematic-representation-of-chemical-vapor-deposition-CVD-process-a-Simplified-scheme_fig2_303501822 (accessed Apr. 28, 2023).
[21] K. A. Shah and B. A. Tali, “Synthesis of carbon nanotubes by catalytic chemical vapour deposition: A review on carbon sources, catalysts and substrates,” *Mater. Sci. Semicond. Process.*, vol. 41, pp. 67–82, Jan. 2016, doi: 10.1016/j.mssp.2015.08.013.
[22] J. Sengupta and C. Jacob, “The effect of Fe and Ni catalysts on the growth of multiwalled carbon nanotubes using chemical vapor deposition,” *J. Nanoparticle Res.*, vol. 12, no. 2, pp. 457–465, Feb. 2010, doi: 10.1007/s11051-009-9667-1.
[23] A. Szabó, C. Perri, A. Csató, G. Giordano, D. Vuono, and J. B. Nagy, “Synthesis Methods of Carbon Nanotubes and Related Materials,” *Materials*, vol. 3, no. 5, pp. 3092–3140, May 2010, doi: 10.3390/ma3053092.
[24] DU, Kang, CHEN, Xuyuan, and ØHLCKERS, Per Alfred, “Direct growth cross linked carbon nanotubes on microstructured metal substrate for supercapacitor application,” WO 2022/078759 A1, Apr. 21, 2022
[25] S. M. Kim *et al.*, “Evolution in Catalyst Morphology Leads to Carbon Nanotube Growth Termination,” *J. Phys. Chem. Lett.*, vol. 1, no. 6, pp. 918–922, Mar. 2010, doi: 10.1021/jz9004762.
[26] X.-D. Wang, K. Vinodgopal, and G.-P. Dai, “Synthesis of Carbon Nanotubes by Catalytic Chemical Vapor Deposition,” in *Perspective of Carbon Nanotubes*, H. El-Din Saleh and S. Moawad Mohamed El-Sheikh, Eds., IntechOpen, 2019. doi: 10.5772/intechopen.86995.
[27] M. Endo, T. Hayashi, Y. A. Kim, and H. Muramatsu, “Development and Application of Carbon Nanotubes,” *Jpn. J. Appl. Phys.*, vol. 45, no. 6A, pp. 4883–4892, Jun. 2006, doi: 10.1143/JJAP.45.4883.
[28] M. Ahmad and S. R. P. Silva, “Low temperature growth of carbon nanotubes – A review,” *Carbon*, vol. 158, pp. 24–44, Mar. 2020, doi: 10.1016/j.carbon.2019.11.061.
[29] V. S. Angulakshmi, S. Karthikeyan, and P. S. S. Shabudeen, “EFFECT OF SYNTHESIS TEMPERATURE ON THE GROWTH OF MULTIWALLEDED CARBON NANOTUBES FROM ZEAMAYS OIL AS EVIDENCED BY STRUCTURAL, RAMAN AND XRD ANALYSES,” vol. 8, 2015.
[30] F. Shamoradi, M. Panjepour, R. Emadi, and M. Ghiaci, “An investigation into the effect of polyvinylpyrrolidone on the size and distribution of nickel catalyst particles for controlling CNTs’ morphology and growth mechanisms in fabricated hybrid CF-CNT nanocomposite,” *Appl. Phys. A*, vol. 129, no. 2, p. 153, Feb. 2023, doi: 10.1007/s00339-023-06443-1.

[31] A. M. K. Esawi, K. Morsi, A. Sayed, M. Taher, and S. Lanka, “Effect of carbon nanotube (CNT) content on the mechanical properties of CNT-reinforced aluminium composites,” *Compos. Sci. Technol.*, vol. 70, no. 16, pp. 2237–2241, Dec. 2010, doi: 10.1016/j.compscitech.2010.05.004.
[32] J. Wang, B. Shen, M. Lan, D. Kang, and C. Wu, “Carbon nanotubes (CNTs) production from catalytic pyrolysis of waste plastics: The influence of catalyst and reaction pressure,” *Catal. Today*, vol. 351, pp. 50–57, Jul. 2020, doi: 10.1016/j.cattod.2019.01.058.
[33] “Thin Film Processing Method - Part 1,” Jun. 11, 2020. https://dracula-technologies.com/thin-film-processing-method-1/ (accessed May 18, 2023).
[34] M. Scimeca, S. Bischetti, H. K. Lamsira, R. Bonfiglio, and E. Bonanno, “Energy Dispersive X-ray (EDX) microanalysis: A powerful tool in biomedical research and diagnosis,” *Eur. J. Histochem.*, Mar. 2018, doi: 10.4081/ejh.2018.2841.
[35] J. Madejová, “FTIR techniques in clay mineral studies,” *Vib. Spectrosc.*, vol. 31, no. 1, pp. 1–10, Jan. 2003, doi: 10.1016/S0924-2031(02)00065-6.
[36] A. J. Hart and A. H. Slocum, “Rapid Growth and Flow-Mediated Nucleation of Millimeter-Scale Aligned Carbon Nanotube Structures from a Thin-Film Catalyst,” *J. Phys. Chem. B*, vol. 110, no. 16, pp. 8250–8257, Apr. 2006, doi: 10.1021/jp055498b.
[37] N. Tripathi, P. Mishra, H. Harsh, and S. S. Islam, “Fine-tuning control on CNT diameter distribution, length and density using thermal CVD growth at atmospheric pressure: an in-depth analysis on the role of flow rate and flow duration of acetylene (C2H2) gas,” *Appl. Nanosci.*, vol. 5, no. 1, pp. 19–28, Jan. 2015, doi: 10.1007/s13204-013-0288-8.
[38] D. He and J. Bai, “Acetylene-Enhanced Growth of Carbon Nanotubes on Ceramic Microparticles for Multi-Scale Hybrid Structures,” *Chem. Vap. Depos.*, vol. 17, no. 4–6, pp. 98–106, Jun. 2011, doi: 10.1002/cvde.201006878.
[39] S. M. TOUSSI, A. F. L-RAZI, A. L. CHUAH, and A. R. SURAYA, “Effect of Synthesis Condition on the Growth of SWCNTs via Catalytic Chemical Vapour Deposition,” *Sains Malays. 4032011 197–201*.
[40] R. Smajda *et al.*, “Synthesis and mechanical properties of carbon nanotubes produced by the water assisted CVD process: Synthesis and mechanical properties of CNTs produced by water assisted CVD,” *Phys. Status Solidi B*, vol. 246, no. 11–12, pp. 2457–2460, Dec. 2009, doi: 10.1002/pssb.200982269.
[41] J. S. C. Kim, “The Role of Hydrogen in the Growth of Carbon Nanotubes: A Study of the Catalyst State and Morphology”.
[42] H.-C. Wen, K. Yang, K.-L. Ou, W.-F. Wu, R.-C. Luo, and C.-P. Chou, “Carbon nanotubes grown using cobalt silicide as catalyst and hydrogen pretreatment,” *Microelectron. Eng.*, vol. 82, no. 3–4, pp. 221–227, Dec. 2005, doi: 10.1016/j.mee.2005.07.028.
[43] V. Ţucureanu, A. Matei, and A. M. Avram, “FTIR Spectroscopy for Carbon Family Study,” *Crit. Rev. Anal. Chem.*, vol. 46, no. 6, pp. 502–520, Nov. 2016, doi: 10.1080/10408347.2016.1157013.
[44] A. B. Suriani *et al.*, “Effect of synthesis time on carbon nanotubes growth from palm oil as carbon source by thermal chemical vapor deposition method,” in *2012 IEEE International Conference on Electronics Design, Systems and Applications (ICEDSA)*, Kuala Lumpur, Malaysia: IEEE, Nov. 2012, pp. 18–21. doi: 10.1109/ICEDSA.2012.6507792.

[45] R. Chen, R. Poon, R. P. Sahu, I. K. Puri, and I. Zhitomirsky, “MnO_2-Carbon Nanotube Electrodes for Supercapacitors with High Active Mass Loadings,” *J. Electrochem. Soc.*, vol. 164, no. 7, pp. A1673–A1678, 2017, doi: 10.1149/2.1491707jes.
[46] K. Hata, D. N. Futaba, K. Mizuno, T. Namai, M. Yumura, and S. Iijima, “Water-Assisted Highly Efficient Synthesis of Impurity-Free Single-Walled Carbon Nanotubes,” *Science*, vol. 306, no. 5700, pp. 1362–1364, Nov. 2004, doi: 10.1126/science.1104962.
[47] A. Magrez, J. W. Seo, R. Smajda, M. Mionić, and L. Forró, “Catalytic CVD Synthesis of Carbon Nanotubes: Towards High Yield and Low Temperature Growth,” *Materials*, vol. 3, no. 11, pp. 4871–4891, Nov. 2010, doi: 10.3390/ma3114871.
[48] D. N. Futaba, K. Hata, T. Yamada, K. Mizuno, M. Yumura, and S. Iijima, “Kinetics of Water-Assisted Single-Walled Carbon Nanotube Synthesis Revealed by a Time-Evolution Analysis,” *Phys. Rev. Lett.*, vol. 95, no. 5, p. 056104, Jul. 2005, doi: 10.1103/PhysRevLett.95.056104.
[49] G. Lota, K. Fic, and E. Frackowiak, “Carbon nanotubes and their composites in electrochemical applications,” *Energy Environ. Sci.*, vol. 4, no. 5, p. 1592, 2011, doi: 10.1039/c0ee00470g.

List of Tables and Figures

Appendix

5.1 Appendix: Sample and $NiSO_4$ solution preparation setup

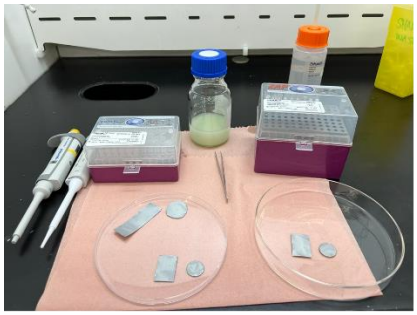

Sample Preparation Inside Fume Hood

Ultrasonic bath

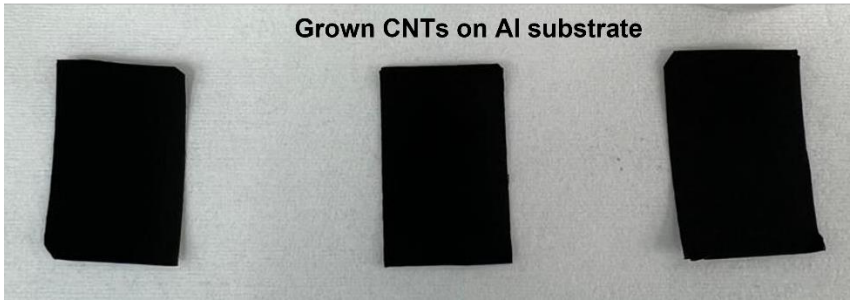

5.2 Appendix: Characterization tools

SEM

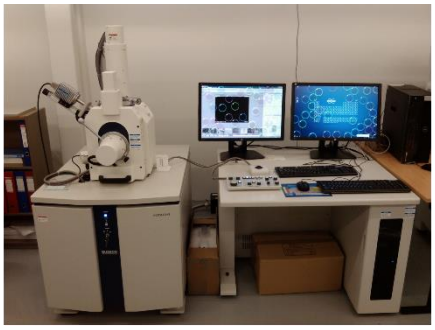

FESEM

FTIR

Scale